



Sintered Bottom and Vitrified Silica Ashes Derived from Incinerated Municipal Solid Waste as Circular Economy-Friendly Partial Replacements for Cement in Mortars

D. A. Wijesekara¹ · P. Sargent² · D. J. Hughes¹ · C. J. Ennis³

Received: 16 May 2023 / Accepted: 8 November 2023 / Published online: 19 December 2023
© The Author(s) 2023

Abstract

Sintered bottom ash (SBA) and vitrified ash (VA) derived from the incineration of municipal solid waste (MSW) at 1200 °C were used in this study as replacements for Type 2 Portland cement (CEM-II) based mortars. This approach negates the need to send them to landfill, benefits the circular economy and contributes towards the decarbonisation of cementitious construction materials in response to international net zero carbon emission agendas. The material (physico-chemical) characteristics of VA and SBA were analysed before being used as partial replacements for CEM-II in mortars, whereby compressive strength (CS) was the primary criterion for assessing engineering performance. VA and SBA replaced CEM-II at dosages of 10%, 25% and 50% based on their high inorganic and pozzolanic contents; whereby the 10% and 25% replacements did not compromise mortar strength. The alkalinity and pozzolanic properties of SBA collectively indicated it has greater potential as a cementitious material over VA, which possessed a neutral pH. The 28-day CS recorded for mixtures containing 25% VA and 10% SBA were 13.74 MPa and 11.77 MPa, respectively compared with 17.06 MPa for CEM-II control samples. The use of 2% additional water in 25% SBA mortar designs improved strength further, indicating that SBA's water retention properties permitted further hydration and strength development with curing. Microstructural, mineralogical and infrared spectroscopy analyses indicated that these strengths were owed to the formation of silicate-based hydration products. The outcomes from this study highlight that SBA has potential for replacing CEM-II and VA as a filler in cementitious mortar.

✉ D. A. Wijesekara
d.wijesekara@tees.ac.uk

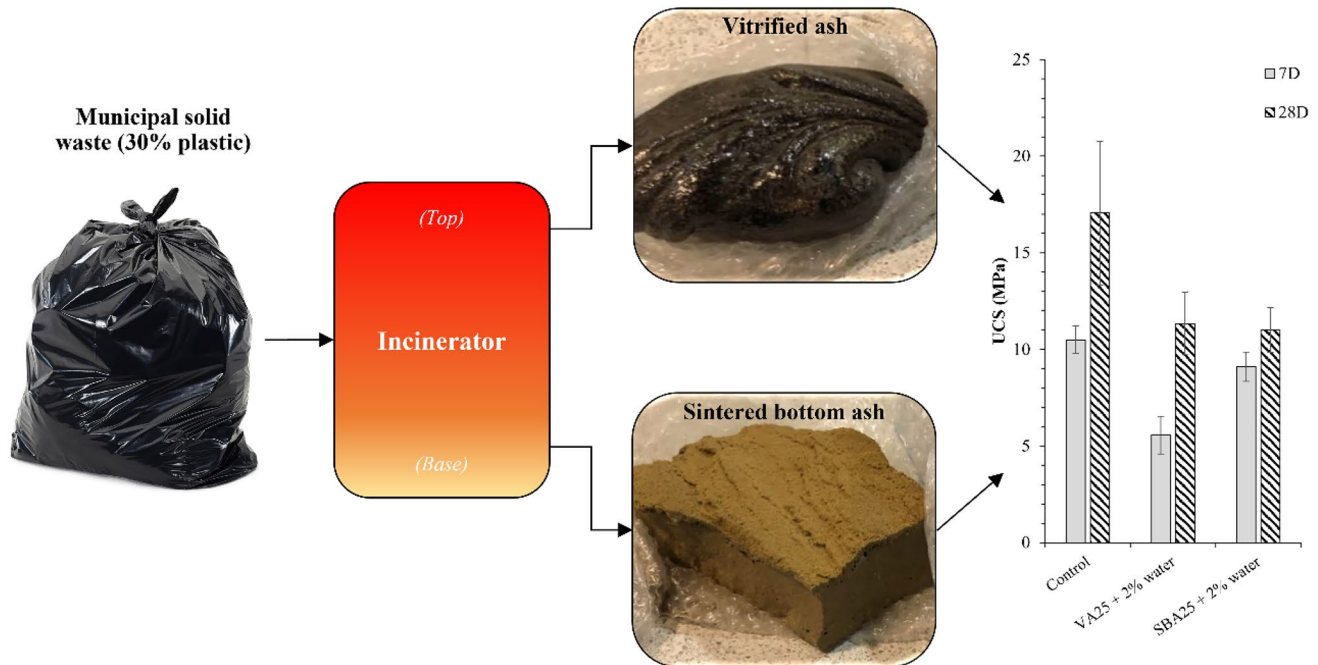
✉ P. Sargent
p.sargent@ulster.ac.uk

D. J. Hughes
d.j.hughes@tees.ac.uk

C. J. Ennis
c.ennis@tees.ac.uk

- ¹ Stephenson Building, School of Computing, Engineering and Digital Technologies, Teesside University, Middlesbrough, Tees Valley TS1 3BX, UK
- ² Belfast School of Architecture and the Built Environment, Faculty of Computing, Engineering and the Built Environment, Ulster University, 2-24 York Street, Belfast, County Antrim BT15 1AP, UK
- ³ Centuria South, School of Health and Life Sciences, Teesside University, Middlesbrough, Tees Valley TS1 3BX, UK

Graphical Abstract



Keywords Sintered bottom ash · Vitrified ash · Circular economy · Municipal solid waste · Cement · Mortar

Abbreviations

Aft	Ettringite
ATR	Attenuated total reflection
CEM-I	Type 1 Portland cement
CEM-II/A-L 32,5R	Type 2 Portland cement (6–20% limestone and 80–94% clinker)
CS	Compressive strength
CSW	CEM-II, sand and water
EDX	Energy dispersive X-ray analysis
E_{\max}	Maximum Young's modulus
FTIR	Fourier transform infra-red analysis
GGBS	Ground granulated blast furnace slag
IBA	Incinerator bottom ash
LOI	Loss on ignition
MK	Metakaolin
MSW	Municipal solid waste
PFA	Pulverised fly ash
SBA	Sintered bottom ash
SCM	Supplementary cementitious materials
SEM	Scanning electron microscope
TGA	Thermal gravimetric analysis
VA	Vitrified ash
XRD	X-ray diffraction

Statement of novelty

The novelty of this study is centred around the application of sintered bottom and vitrified ashes derived from municipal solid waste incineration, as supplementary replacements for Portland cement in mortars. Through mortar design optimisation, 28-day compressive strengths of up to 13 MPa were achieved. Engineering performance testing, along with mineralogical and microstructural surveys indicated that sintered bottom ash had better prospects as a cementitious binder, whereas vitrified ash better served as a fine-grained siliceous aggregate. These findings collectively provide circular economy-friendly solutions for future cementitious mortar design.

Introduction

Global cementitious material consumption has increased annually since 2012, owing to accelerating rates of urbanisation. Type 1 Portland cement (CEM-I) manufacture is expected to increase from 2.77 Gt in 2007 to 4.6 Gt in 2050 [1]. For a European cement plant, the thermal energy requirement is 3.75 MJ per tonne of clinker [2]. Globally, CEM-I production contributes 8–10% of total

CO₂ emissions [3]; whereby 1 tonne of CEM-I production generates 761–830 kg of CO₂ [4]. The United Nations Environmental Program Sustainable Building and Climate Initiative suggested the following approaches for reducing the environmental footprint of cement manufacture: (1) alternative clinker materials, (2) improved energy efficiency, (3) increased use of renewable energy sources and (4) increased use of pozzolanic mineral wastes and by-products as supplements or replacements for CEM-I [5]. Research into low carbon construction materials that utilise readily available pozzolanic industrial and municipal wastes is highly topical, especially since the publication of UN Sustainability Development Goals and international governmental agendas for achieving net-zero carbon emissions by 2050. Examples of supplementary cementitious materials (SCM) that are widely used in cementitious mortars include ground granulated blast furnace slag (GGBS) and pulverised fly ash (PFA).

Mechanical strength is one of the primary criteria that dictates the level of CEM-I replacement within mortars. Hence, knowledge of an SCM's pozzolanic activity is crucial as it defines the availability of siliceous and/or aluminous compounds to react with Ca(OH)₂ and water to form hydration products. Strength development within mortars is also attributed to their packing characteristics, as a function of the texture of aggregates and binders. Goldman and Bentur [6] suggested that the 'micro-filler effect' of SCMs plays an equal or even larger role in strength development compared with cementitious hydrates.

The continued dependence on PFA and GGBS as SCMs is unsustainable. PFA availability is declining due to the closure of coal-fired power stations, as part of the global effort in reverting from fossil fuels to renewable energy sources for generating electricity. Furthermore, iron and steel-making markets have shrunk considerably since the 1990's across the UK and Europe, as have GGBS supplies as a consequence. Hence, the UK amongst other European nations now import PFA and GGBS from overseas, which further increases the economic and environmental costs of construction projects. This serves as motivation for investigating low-value large-volume waste streams as SCMs, which would be an environmentally sustainable waste management solution that negates their disposal to landfill.

One of the world's largest waste streams with reliable supplies all-year-round is municipal solid (bin-liner) waste (MSW), which has traditionally been disposed to landfill. However, since the early 2000's energy-from-waste technology has become a viable eco-friendly solution for processing MSW, involving incineration at 850 °C [7] whilst generating electricity for feeding into national power grids. Energy-from-waste markets have steadily grown across the UK, Europe and the USA. Between 1990 and 2021, the

UK's production of bioenergy and waste as 'primary fuels' increased from 0.7 to 12.8 million tonnes of oil equivalent [8].

Incineration typically produces incinerator bottom ash (IBA), which accounts for ~80% (by total weight) amongst other solid effluents comprising different constituents such as glass cullet, ceramics, slag/sintered phases and incom-bustible materials depending on feedstock composition [9–11]. IBA is commonly pozzolanic, albeit heterogeneous with variable quantities of inorganic metals, glass, ceramics and residual organic matter. Tang et al. [9] determined that whilst variations in IBA composition had negligible effects on the CS of CEM-I-based mortars, IBA with high fines (< 125 µm) content adversely impacted cement hydration (by absorbing free water) and reduced CS by 20–50%. Subsequently, Tang et al. [12] investigated the role of various IBA constituents (e.g. broken glass cullet, ceramics, sintered low and high ferrous slags) on CS; whereby IBA's containing powdered glass and ceramics produced higher CS performances.

To date, the most common application for IBA has been aggregates for concrete and pavement sub-bases [12]. Thenarasan Latha et al. [13] and Abinaya and Balasubramanian [14] stabilised MSW based BA and FA in compressed earth blocks. However, IBA may also be used as an SCM given its pozzolanic reactivity and calcium content. Yang et al. [15] assessed MSW-derived ashes as SCMs at replacement dosages of 10–50 wt.%. Relative CS of cement composites comprising 30 wt.% MSW ash and 30 wt.% IBA were 66% and 43% higher, respectively compared with control mixtures. However, some studies have reported that IBA retards hydration, thereby reducing strength and increasing leachability [15–17]. Caprai et al. [17] observed that the CS of cement pastes decreased by 52% as CEM-I replacement with IBA increased from 10 to 50%.

High temperature sintering (> 1200 °C) and vitrification can convert residual IBA wastes into more environmentally benign materials; from loosely bound fine particles into solid consistent masses. Hence, the leachability of hazardous elements (e.g. Cl, Pb, As, Cd, Hg, Mo and Sb) is reduced [18, 19]. Thus, sintered bottom ash (SBA) and vitrified ash (VA) have valorisation potential as SCMs.

Research on the use of thermally treated ashes such as VA and SBA as aggregates or SCMs in mortar is very limited [20–22]. Hence, this study aims to fill this knowledge gap by developing a new generation of circular economy-friendly cementitious mortars that valorise pozzolanic MSW-derived SBA and VA as SCMs. Key relationships will be established between the physico-chemical properties of SBA and VA, the mechanical strength, mineralogy and microstructure of composite mortar mixtures, with a view to identifying the maximum permissible level of replacement for CEM-II, whilst retaining its design strength properties.

Materials and Testing Methodologies

Mortar Constituents

Due to better availability, lower unit cost and lower carbon print (up to 16%) compared with Type 1 Portland cement (CEM-I) [23], Type 2 Portland-limestone cement (CEM-II/A-L 32,5R) was used as the binder for manufacturing control mortar samples. CEM-II was sourced from Tarmac Cement and Lime Ltd (Birmingham, UK), which comprised 6–20% limestone and 80–94% clinker to produce 2-day CS \geq 10 MPa and 28-day CS of 32.5–52.5 MPa (in accordance with EN 197–1 [24]).

SBA and VA residues were provided by Renewable Energy Waste Solutions UK Plc (REWS), which were generated from the incineration of MSW; whereby the feedstock used was (household) black bin bags (containing approximately 30% plastic). Prior to incineration, the MSW was sorted, shredded and dried within a vertical air jet mill. Subsequently, the waste was transferred to a chain conveyer dryer to achieve a moisture content $<$ 10%. 2/3 of the material was then transferred to the incinerator. The system required an ‘input’ heat source of 450 °C to pre-heat the incinerator from its base, which eventually reached an operating temperature of 1200 °C. Incorporated within the incinerator system was a high-temperature cyclone, which served as a gas-particulate separator to reduce the ash and char content of the generated syngas. The high-temperature syngas ‘output’ was then used to power a separate pyrolysis plant, to which the remaining 1/3 of the dried MSW was fed. Once the incinerator had reached the required operating temperature and was

processing MSW, black-coloured glassy vitrified ash (VA) was siphoned from the ‘output end’ (top) of the incinerator, whereas a brown-coloured sintered bottom ash (SBA) was collected from its base. A summary of this treatment process is presented in Fig. 1.

The raw forms of the SBA and VA residues were akin to soft rocks. Hence, for ease of sample mixing and maximising homogeneity for sample manufacture, they were manually broken down into gravel-sized particles by using a hammer and then pulverised in a disc mill. The milled residues were then passed through a 150 μ m sieve to produce particle size distributions (PSD) for VA and SBA that were comparable with CEM-II, given that particle sizes for CEM-II are generally 7–200 μ m [25, 26].

The fine aggregate component of mortar samples comprised sand, which complied with BS EN 12620 + A1 [27] and was sourced from Tarmac Building Products Ltd (Wolverhampton, UK).

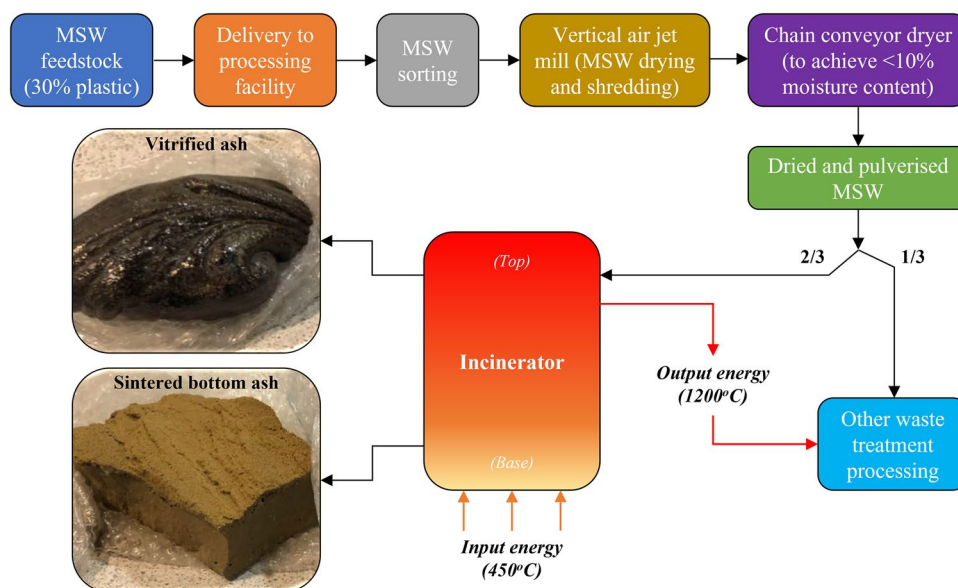
For pozzolanic activity testing, metakaolin (MK) was sourced from Sigma Aldrich (Germany) for use as the standard reference material (CAS No. 1332-58-7). The MK was commercially produced by calcining Kaolin ($\text{Al}_2\text{Si}_2\text{O}_5(\text{OH})_4$) at 850 °C.

Testing Methods

Residue Characterisation

The PSD’s for SBA and VA residues were determined in accordance with BS 1377–2 [28] through dry sieving, whereby the sieve sizes used ranged between 150 and 63 μ m. Numerous physico-chemical properties of the SBA and VA

Fig. 1 Schematic of the treatment stages used to process municipal black bin bag waste for syngas energy generation and subsequent pyrolysis



were assessed, including pH, loss on ignition (LOI), thermal gravimetric analysis (TGA) and pozzolanic activity. For pH testing, the procedure involved adding 1 g samples of SBA and VA to a 250 cm³ HDPE bottle containing 20 cm³ of deionized water. The bottle was subsequently shaken using an orbital shaker at 100 rpm for 30 min. The mixed solutions were then filtered using Whatmans no.1 paper, whereby their pH values were measured using Hanna Instruments HI8519 N microprocessor pH/mV benchmeter.

LOI testing was performed at 830 °C for 3-h to determine the organic matter content of the SBA and VA. To determine their composition and thermal stability, TGA was performed in accordance with ASTM E1131-20 (ISO 11358) [29], using a PerkinElmer Simultaneous Thermal Analyzer, STA 6000. Samples of 50 ± 5 mg were heated from 30 to 1000 °C, using a heating rate of 20 °C min⁻¹ and a nitrogen flow rate of 40 cm³ min⁻¹.

The pozzolanic activities of the SBA and VA residues were assessed using the ‘saturated lime’ and Frattini tests. Figure 2 summarises the reactions and testing procedures for both methods, which were broadly similar. For saturated lime testing, test solutions were prepared by dissolving 2.0 g of Ca(OH)₂ in 1000 cm³ of deionised water. A 75.0 cm³ saturated lime solution was placed in a plastic bottle for the control sample, whereas 1.0 g of VA or SBA was added to the solution to form test samples. Samples were then stored in an oven at 40 °C for 1, 3, 7, and 28 days. For each period, samples were removed from the oven, cooled and subjected to vacuum filtration. Filtrates were analysed for [OH⁻] by titrating against 0.1 M HCl with a methyl orange indicator. The pH of the titrated solution was then adjusted to 12.5 by adding NaOH pellets and analysed for [Ca²⁺] by titrating against 0.06 M EDTA solution with Patton and Readers

indicator. Given that the initial Ca(OH)₂ content of samples was known, the quantity of Ca²⁺ and OH⁻ consumed by the pozzolan could then be quantified [30].

For Frattini testing, 20 g samples comprising 80% CEM-II and 20% of either VA or SBA were placed in a plastic bottle containing 100 cm³ of deionised water, which were then stored in an oven at 40 °C for 8-days. Samples were then cooled, filtered using vacuum filtration and the resulting filtrate was analysed for [OH⁻] through titration against 0.1 M HCl with a methyl orange indicator. The pH of the titrated solution was adjusted as for the ‘saturated lime method’. Results were then presented such that [Ca²⁺] was expressed as equivalent [CaO] (mmol) vs remaining [OH⁻] (mmol). Data points that plot below the solubility curve for Ca(OH)₂ indicate removal of Ca²⁺— indicative of pozzolanic activity. Contrastingly, data points plotting on or above the solubility curve indicate zero pozzolanic activity. This approach was based on the assumption that no other sources of calcium were present in the mortar mixtures other than CEM-II [31].

Mechanical Strength

Two stages of CS testing were performed: ‘Stage 1’ assessed control (CEM-II) and hybrid mortar mixtures (i.e. CEM-II replaced with 10%, 25% and 50% of SBA or VA, based on BS EN 197–1 criteria [24]). A summary of the sample mixtures considered is presented in Table 1. ‘Stage 2’ was informed by the outcomes of Stage 1, whereby for the most effective level(s) of CEM-II replacement with SBA and VA in terms of strength development, additional mortar mixtures were prepared containing an extra 2% water (relative to the overall mortar mass) to investigate whether this would promote further hydration and strength gains.

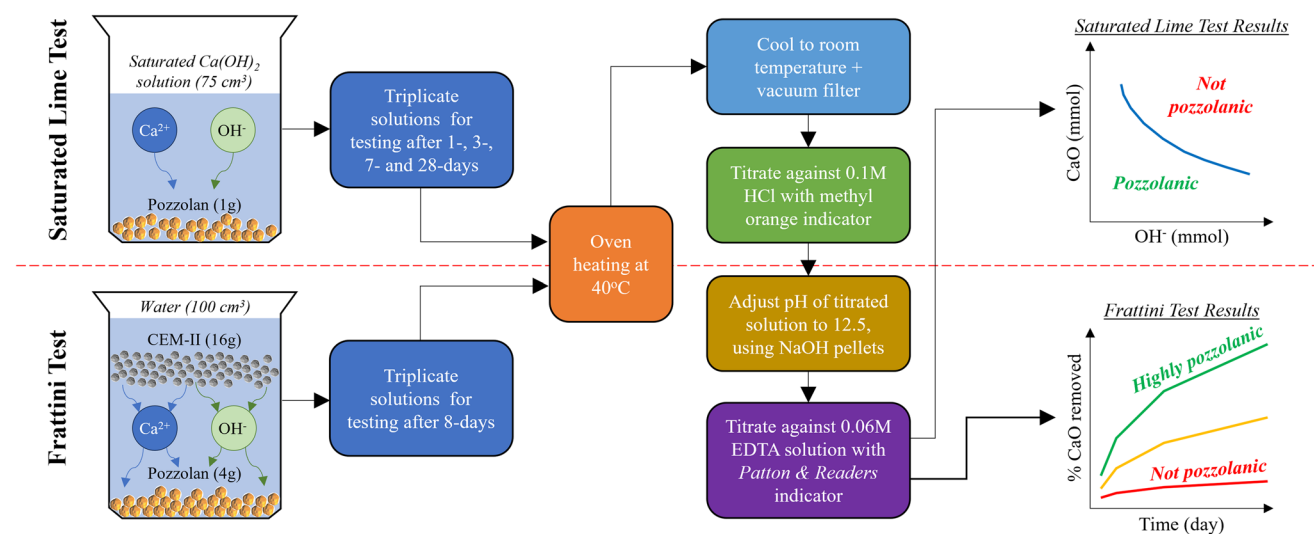


Fig. 2 Flow diagram of experimental procedures for Saturated Lime and Frattini tests

Table 1 Summary of mortar designs assessed with corresponding sample mass and density information

Sample ID	Residue used	Percentage replacement of CEM-II with residue	Sample condition after 1-day upon demoulding		Sample condition after 7-days		Sample condition after 28-days	
			Ave. mass (g)	Ave. density (kg/m ³)	Ave. mass (g)	Ave. density (kg/m ³)	Ave. mass (g)	Ave. density (kg/m ³)
Control	None	0	605.79	2366	584.99	2285	576.99	2254
SBA10	SBA	10	606.50	2369	586.00	2289	578.00	2258
SBA25	SBA	25	607.57	2373	586.67	2292	578.67	2260
SBA50	SBA	50	609.70	2382	588.70	2300	580.70	2268
VA10	VA	10	609.56	2381	588.72	2301	580.72	2264
VA25	VA	25	615.21	2403	593.54	2319	585.54	2287
VA50	VA	50	624.64	2440	604.64	2362	596.64	2331

**Fig. 3** Prism mortar samples after demoulding

Sample Preparation Triplicate cuboidal (prism) mortar samples (40 mm×40 mm×160 mm) were prepared in accordance with BS EN 196–1:2016 [31], whereby mixtures comprised sand to cement ratio of 3:1 and cement to water ratio of 2:1. The dried cementitious binders (i.e. CEM-II, SBA and VA) were placed in a mechanical mixer for 5 min at 60 rpm. Subsequently, water was added to the mixture and mixed for a further 5 min at the same mixing speed. The sand was then added and mixed for a further 5 min to produce a homogenous mortar. Once mixed, the mortar was cast into moulds and wrapped in thin polyethylene film for curing at ambient air temperature (20 °C at ~50% relative humidity) for 22 ± 2 h. Samples were then demoulded and placed in a water bath (20 °C) for 7- and 28-days curing before CS testing. A summary of the sample information is provided in Table 1, with an image of demoulded mortar samples provided in Fig. 3.

Compressive Strength (CS) Prior to testing, samples were trimmed to size (if necessary) — ensuring that end faces were parallel with each other. CS tests were performed using an Instron 3367 loading frame in accordance with BS

1377-2 [28], whereby a constant strain rate of 1.27 mm/min was used to gain detailed insights into the deformational behaviour of the new VA and SBA based mortars.

Microstructure and Mineralogy

The mineralogical composition of CEM-II, SBA, VA and cured composite mortar samples were analysed through X-ray diffraction (XRD). The apparatus used was a Siemens D5000 Diffractometer (Cu K-alpha radiation of wavelength 0.154 nm, generated by a Cu anode operated at 40 kV and 20 mA). Scans were undertaken over a 2-theta range of 10°–90° with a nominal step size of 0.2 and a scanning rate of 1 per minute. Mineral phase identification was performed using Profex 4.3.6 software.

The microstructure of the residues (post LOI) and cured mortar mixtures were investigated using scanning electron microscopy (SEM), whereby the apparatus used was a Hitachi S–3400N. The bulk elemental composition of the raw materials was analysed with energy dispersive x-ray (EDX) apparatus, which possessed an electron source of pre-centred cartridge type tungsten hairpin filament.

To determine the composition of cementitious precipitates within the cured mortars, sub-samples were taken from CS prisms and subjected to Fourier transform infrared (FTIR) spectroscopy analysis. The apparatus used was a Thermo Scientific TM Nicolet TM iS TM 5 FTIR spectrometer, with a diamond attenuated total reflection attachment, at 1 wavenumber resolution.

Results

Residue Characterisation

PSD, Microstructure, Composition and LOI

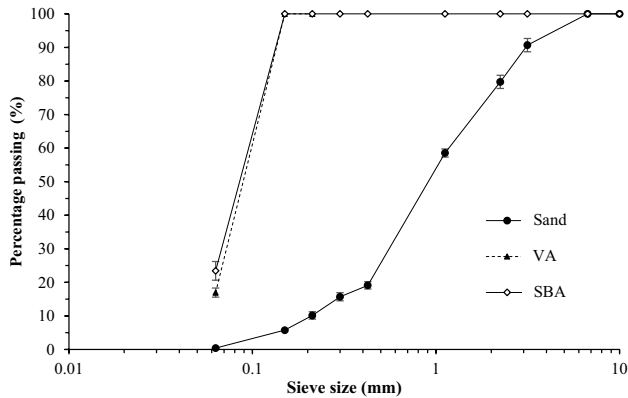


Fig. 4 PSD curves for sand, VA and SBA

PSD curves for the sand, VA and SBA are presented in Fig. 4. Figure 5 shows the visual appearance of the pulverised SBA and VA residue powders, along with SEM micrographs that highlight their microstructure and particle morphologies. SBA was a powdery residue while VA consisted of glass like shard particles as a result of the vitrification process.

Pulverisation increased sharp angular particulate content for VA compared with SBA, as observed in Fig. 5c and d. Moreover, the higher fines content of both residues resulting from pulverisation promoted improved sample compaction properties when included in mortar mixtures.

Bulk elemental composition and LOI values of the residues are shown in Table 2. It is important to note the Si, Al and Ca content of the residues compared with CEM-II, PFA and GGBS (as popular SCMs), as these elements play a fundamental role in pozzolanic reactions and hydration products formation. LOI values for both residues were $< 0.3\%$ as they were produced at $1200\text{ }^{\circ}\text{C}$, resulting in the combustion of all organics (including aromatics) and chlorides associated with original waste feedstocks; thereby leaving a high ash content [32]. Hence, SBA and VA possessed high pozzolanic

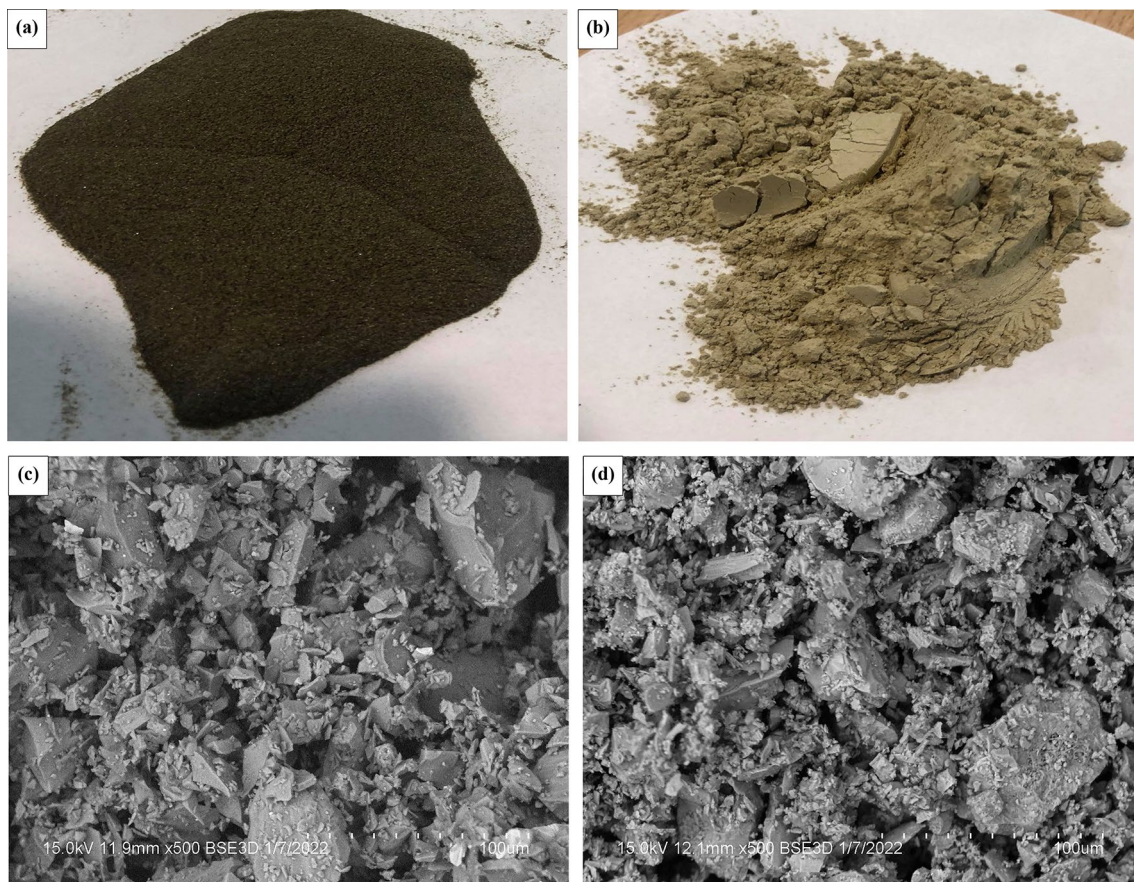


Fig. 5 Visual appearance of pulverised **a** VA and **b** SBA. SEM micrographs showing the microstructural features of pulverised **c** VA and **d** SBA. Note: For scale, images **a** and **b** of filter paper = 10 cm (dia)

Table 2 Summary of LOI values and bulk elemental composition for pulverised SBA and VA residues compared with CEM-II and traditionally used SCMs

Material	LOI (%)	O (%)	Mg (%)	Al (%)	Si (%)	P (%)	S (%)	K (%)	Ca (%)	Na (%)	Ti (%)	Cr (%)	Fe (%)	Zn (%)
SBA	0.24	42.8	1.2	4.9	16.9	0.6	0.2	0.4	25.8	–	1.3	0.18	3.8	1.9
VA	0.26	48.9	2.1	4.2	21.6	0.7	0.1	1.4	12.8	–	1.0	0.20	5.2	1.9
CEM-II	–	51.0	0.6	1.1	4.9	–	–	0.6	40.0	–	–	–	1.82	–
PFA	1.2	–	–	25.0	72.0	–	–	1.2	0.7	3.0	–	<0.1	3.5	<0.1
GGBS	1.0	31.8	3.0	4.2	12.9	–	0.7	0.6	29.9	–	–	–	0.3	–

GGBS data courtesy of Gonzalez et al. [33]; PFA data courtesy of Mahima Kumar et al. [34]

contents (and potentially reactivity), thereby making them potential SCMs.

Whilst the Al content of the SBA and VA were comparable to GGBS, they were significantly lower than for PFA. The Si content of the VA was markedly higher than that for the SBA and GGBS, but significantly less than PFA. If the silicates present within VA were mostly amorphous, it could have promise as a pozzolan [35, 36] and potential for producing long-term high strength gains. However, the Ca content of both the SBA and GGBS were more than double that recorded for the VA. These results suggest that an additional source of alkali (e.g. CEM-II, NaOH, $\text{Na}_2\text{Si}_2\text{O}_5$) may be required in VA-based mixtures to initiate the dissolution of aluminosilicate chains to form new cementitious products and subsequent strength gains.

pH

The pH values measured for the SBA and VA residues were 10.7 and 8.8, respectively. These values were markedly less alkali compared with CEM-II, whose pH was 12.7. Whilst the VA did not possess a sufficiently high pH for pozzolanic reactions (i.e. $\text{pH} \geq 10.5$, as per Davidson et al. [37]), the

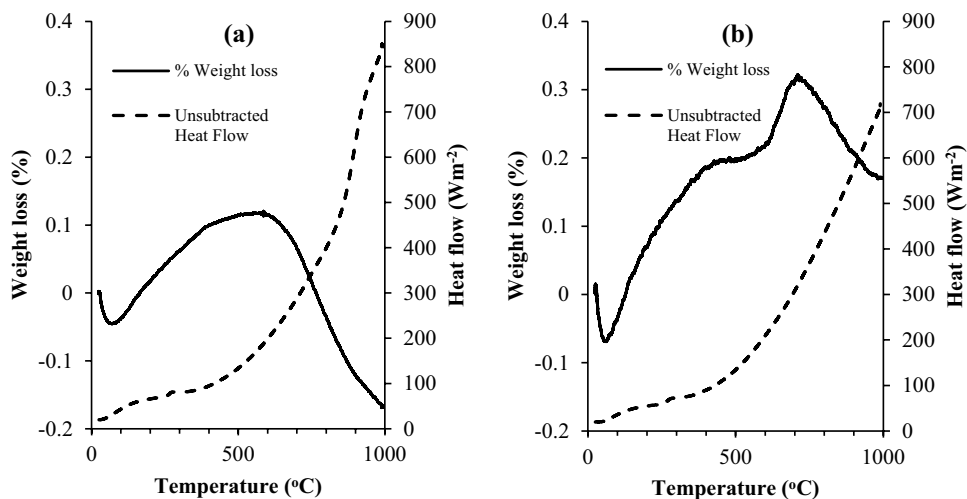
higher Ca contents measured from EDX analyses and higher pH for SBA compared with VA suggests that SBA has more similar chemistry to CEM-II. Overall, SBA has similar physico-chemical properties as GGBS, which is encouraging as GGBS is well known to produce high strength performances when added in cements, concretes and mortars.

TGA

Thermal degradation and stability curves for SBA and VA are shown in Fig. 6. The heat flow observed for both samples was largely consistent, albeit the maximum heat flow at 1000 °C for VA was slightly higher (841 Wm^{-2}) compared with SBA (715 Wm^{-2}). The weight losses observed between 550 °C and 650 °C were due to the pyrolysis of soot in both residues; whereby VA and SBA showed maximum weight losses of 0.11% and 0.31%, respectively.

Whilst the general trend in weight loss with increasing temperature was similar for both VA and SBA up to 600 °C, they exhibited different behaviour for temperatures > 600 °C. The weight loss measured for VA progressively decreased towards a minimum of -0.17% at 1000 °C, whereas the weight loss measured for SBA further increased

Fig. 6 TGA results for the pulverised residues: **a** VA and **b** SBA



up to ~717 °C before decreasing towards 0.17% at 1000 °C. Overall, such weight losses in both residues were considered negligible due to the operating temperature (1200 °C) used in the incinerator.

Pozzolanic Activity

Saturated lime Method The pozzolanic activity of the residues are reported as % CaO removed per gram of test pozzolan after intervals of 1-, 3-, 7- and 28-days, as presented in Fig. 7. Results for MK and control experiments performed by Donatello et al. [30] are also reported to corroborate the results obtained in this study for equivalent samples. The pozzolanic activity of VA and SBA increased from 1- to 28-days.

However, the rate at which CaO was removed from the residues differed; whereby SBA exhibited a near-constant linear increase over the 28-days. Contrastingly, the VA’s

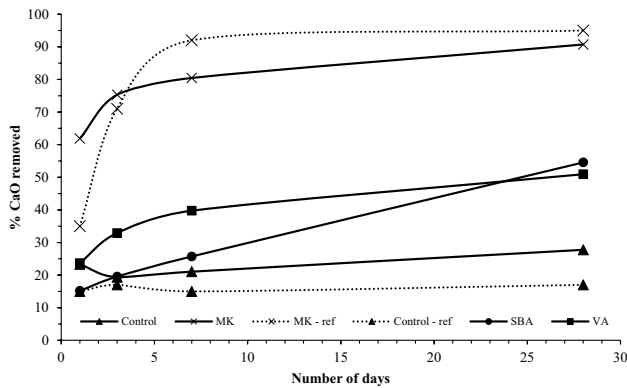
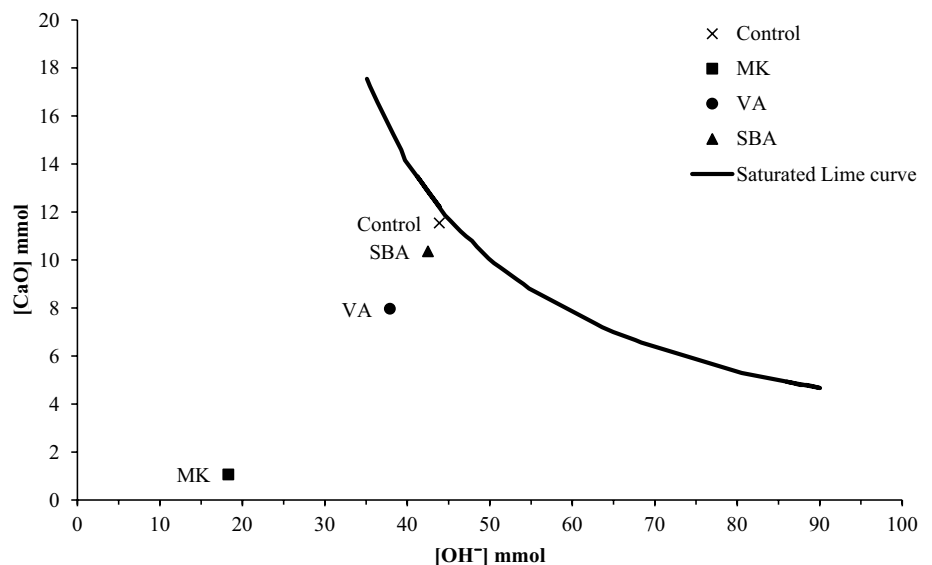


Fig. 7 Saturated lime pozzolanic activity testing results for control, MK, VA and SBA residues

Fig. 8 Frattini test results for test pozzolans VA, SBA, control and MK after 8-days curing at 40 °C



rate of CaO removal exhibited near-logarithmic behaviour — showing significant retardation between 7- and 28-days. After 28 days, SBA achieved a higher degree of CaO removal (55%) than VA (31%).

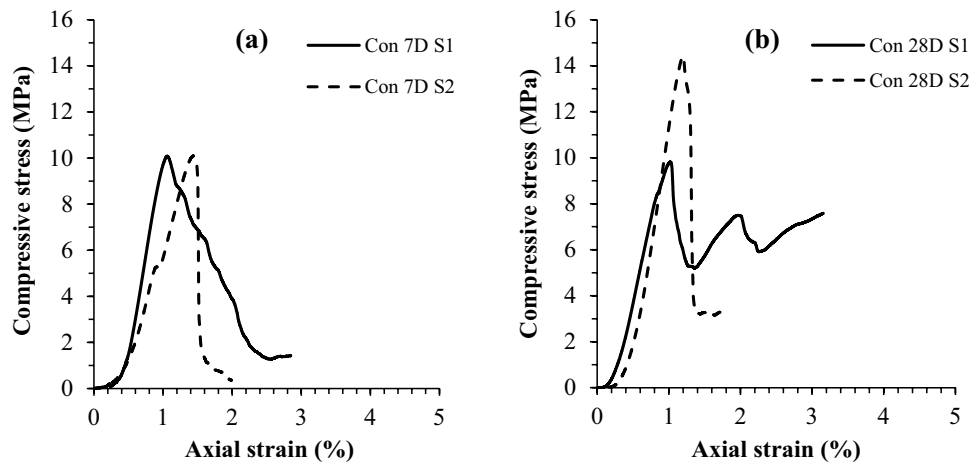
Frattini Test Frattini testing results are reported in Fig. 8 as millimoles of CaO vs OH⁻ ions in solution after 8-days curing at 40 °C. The saturated lime curve is also presented for enabling comparisons. As anticipated, the result for the control sample comprising 100% CEM-II plots on the saturated lime curve. Contrastingly, data points for VA, SBA and MK plot below the curve, indicating removal of Ca²⁺ from the solutions and a reflection of their pozzolanic activity. Based on the relative position of the data points for MK, VA and SBA with respect to the saturated lime curve, MK possessed the highest level of pozzolanic activity, followed by VA and SBA respectively.

For an equivalent curing period of 7- to 8-days, the results obtained from the saturated lime and Frattini testing methods are consistent — indicating that VA possessed higher levels of pozzolanic activity during the early stages of curing. However, at the end of the 28-day testing period for the saturated lime method, the long-term pozzolanic activity of the SBA was superior. This suggests that mortar mixtures containing SBA will more likely achieve higher engineering strengths.

Compressive Strength (CS)

The compressive stress vs axial strain behaviour for control mortar samples after 7- and 28-days curing is shown in Fig. 9. Longer curing time resulted in higher strength development in samples. In general, the mechanical behaviour of samples was characterised by near-linear elasticity at small

Fig. 9 Stress vs strain curves for control mortar mixes after curing for **a** 7-days and **b** 28-days



strains before yielding and reaching their peak compressive stress, when they experienced a brittle failure. Post-peak stress, samples generally exhibited rapid softening behaviour before ultimately approaching residual strength.

Stage 1

The mechanical strength behaviour of mortar samples containing 10, 25 and 50% VA by weight of CEM-II after 7-days and 28-days curing are shown in Fig. 10. 7-day samples containing 10% and 50% VA exhibited more ductile behaviour post-peak stress. Whereas samples containing 25% VA achieved the highest 7- and 28-day CS and exhibited more brittle behaviour upon failure.

The compressive stress–axial strain response of mortar samples containing 10, 25 and 50% CEM-II replacement with SBA after 7- and 28-days curing are presented in Fig. 11. For both curing periods, 10% replacement of CEM-II with SBA generally resulted in a ductile response after peak stress. Using higher levels of CEM-II replacement of 25% and 50% SBA resulted in more elastic brittle failures. However, using 10% SBA produced the highest 28-day CS values; whereby increasing SBA content towards 50% had detrimental effects on strength development.

The CS results and maximum Youngs Modulus (E_{\max}) measurements for the control, VA and SBA-based mortar mixes after 7- and 28-days curing are presented in Figs. 12 and 13, respectively. CS and E_{\max} generally increased over the 28-day period for all mixes regardless of the residue dosage. The 28-day CS and E_{\max} values for control samples were 14.64 MPa and 2.06 GPa respectively. 28-day CS values for mortars comprising 25% VA (13.74 MPa) were similar to those measured for the control mortar. Furthermore, 28-day E_{\max} values measured for control, 10% SBA and 25% VA mortars were relatively consistent, ranging between 2.03 and 2.20 GPa. However, using 50% VA or SBA had a detrimental effect on the 7- and 28-day CS

and E_{\max} values, which were markedly lower than those recorded for mixtures containing 10% VA or SBA.

Based on the CS results and E_{\max} measurements obtained, and this study's objective to replace as much CEM-II as possible in the mortar mixtures, mortars containing 25% replacement with VA and SBA were selected for further investigation. Additional (equivalent) samples were prepared with 2% additional water to assess whether this would promote further hydration and strength gains within the mortars.

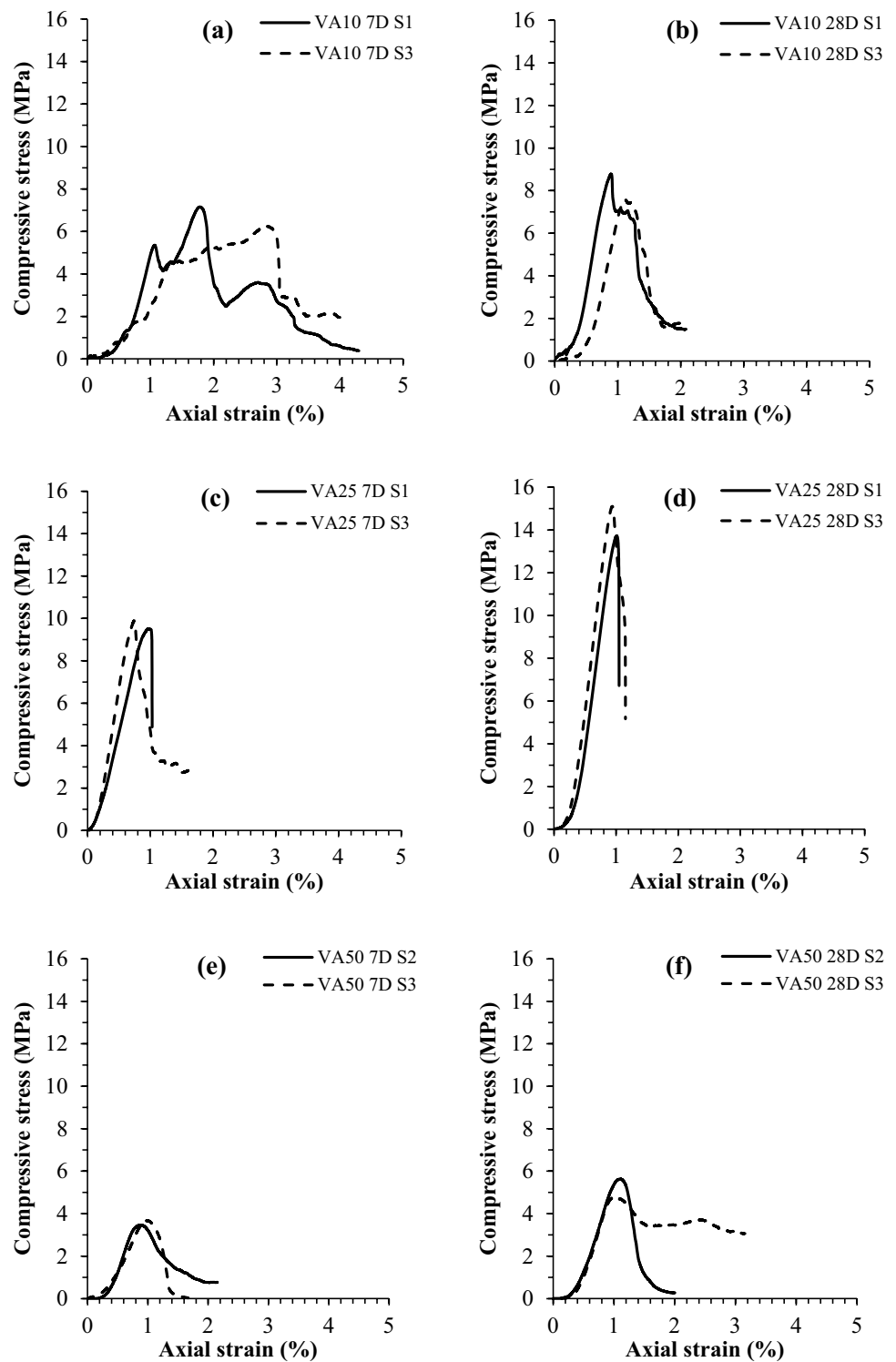
Stage 2

Figure 14 presents the 7- and 28-day compressive stress–axial strain response for the 25% SBA and VA mortar mixes with an additional 2% of water. All samples exhibited brittle failure, with the exception of the 7-day VA25 sample.

The CS results and E_{\max} measurements for the control and the 25% replacement VA and SBA-based mortar mixes after 7- and 28-days curing are presented in Figs. 15 and 16, respectively.

As evident in Figs. 12 and 15, the addition of 2% extra water had opposite effects on the 7- and 28-day strengths recorded for the VA25 and SBA25 mixtures; whereby the former experienced weakening and the latter experienced strengthening. Hence, the addition of 2% water was successful in promoting hydration reactions and strength gains in the 25% SBA-based mortar mixtures. This highlights the potential of adding more water in the SBA10 mixture to produce higher strength gains. Contrastingly, the additional water in the VA25 mixtures will have likely diluted the (already lower) pH of the mortar mixture compared with the control and SBA25 mixtures — thereby compromising pozzolanic activity and long-term strength development.

Fig. 10 Mechanical behaviour of VA-based mortar mixes: 10% replacement at **a** 7-days and **b** 28-days; 25% replacement at **c** 7-days and **d** 28-days; 50% replacement at **e** 7-days and **f** 28-days



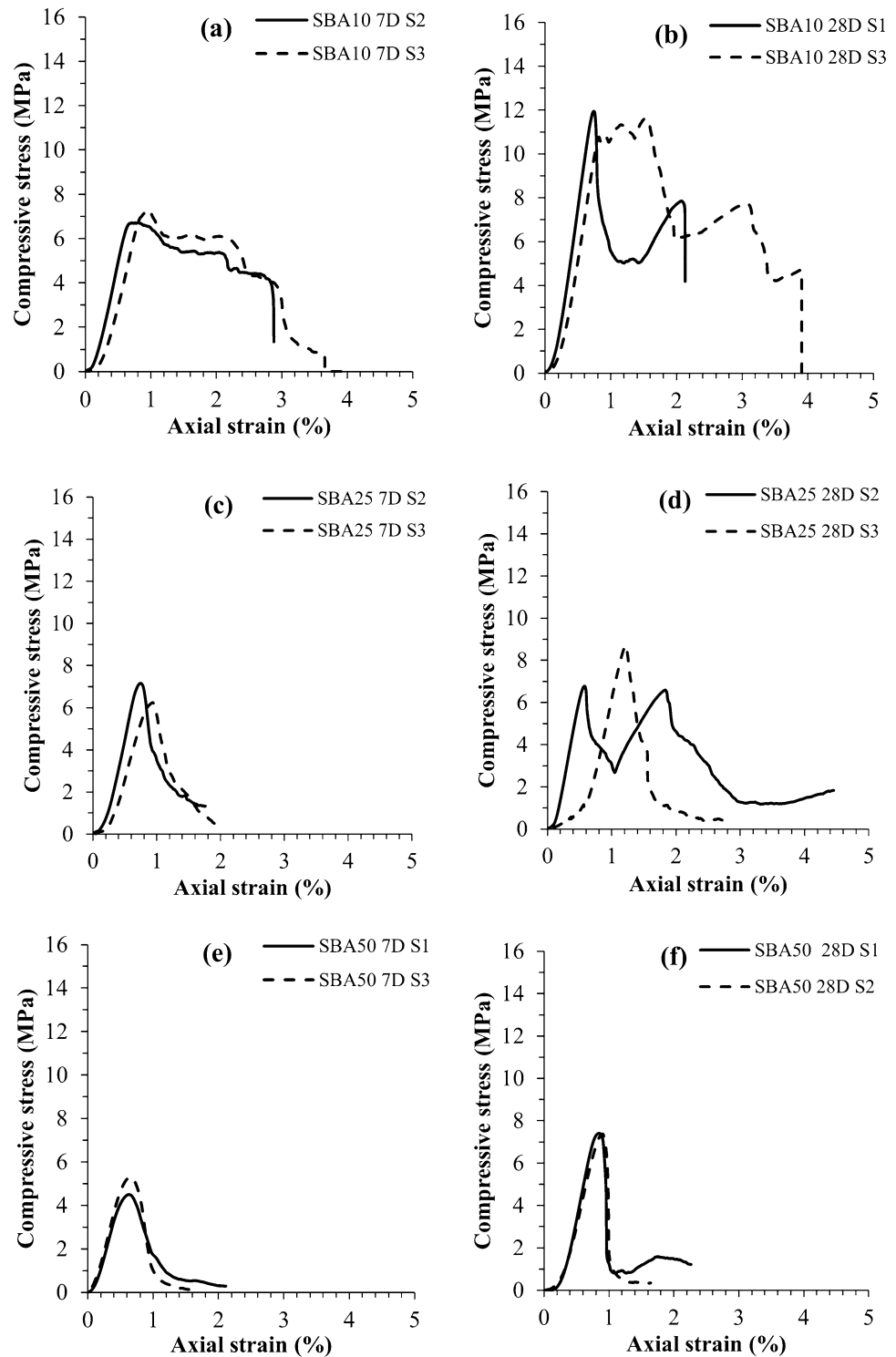
Microstructure and Mineralogy

Microstructure Imaging

The microstructure of the control CEM-II mortars is shown in Fig. 17; whereby in images (a) and (b), the material

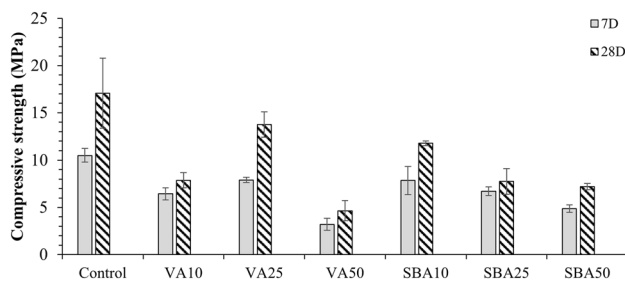
possessed a densely compacted and well cemented microstructure. Occasional open pores were also present, with some evidence of interconnectivity. Furthermore, tabular hexagonal particles were observed throughout the material (Fig. 17c)—notably infilling open pores and adhering to the global exterior surface of the mortar. These

Fig. 11 Mechanical behaviour of SBA-based mortar mixes: 10% replacement at **a** 7-days and **b** 28-days; 25% replacement at **c** 7-days and **d** 28-days; 50% replacement at **e** 7-days and **f** 28-days



hexagonal particles were identified as calcium carbonate/hydroxide (CH) phases. Radiating needle-like growths can be observed in Fig. 17b and d to be infilling void spaces between sand and CEM-II clinker particles. These growths were AFt (Ettringite) phases.

Presented in Fig. 18 are SEM micrographs for 28-day cured mortars containing 10, 25 and 50% replacement of CEM-II with VA and SBA. In general, the range of particle sizes and shapes present within mortars containing 50% replacement with VA and SBA was more diverse compared



Summary of 7-day and 28-day CS performances for control, VA and SBA-based mortar mixtures

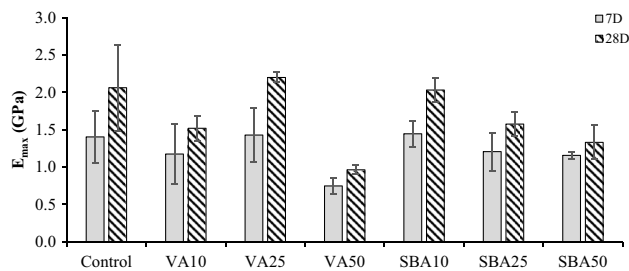


Fig. 13 Summary of 7-day and 28-day E_{max} values for control, VA and SBA-based mortar mixtures

with control, 10% and 25% replaced mortars. Aft needle-like growths could be seen in both VA and SBA-based mortars, infilling void spaces observed in Fig. 18a, b and e. However, the dimensions of the Aft phases appeared to be smaller and less well established compared with observations made for CEM-II control mortars. Hexagonal tabular carbonate minerals were abundant (Fig. 18b), associated with the CEM-II content of the mortar mixtures. However, features which were absent in the control mortar but present in the VA25 mortar specimen were small cubic-like particles (as seen in Fig. 15c). Based on observations made by Liu et al. [38] on similar materials, these were likely to be partially carbonated calcium-rich crystals.

For VA based mixtures (Fig. 18 a, c and e) the amount of granular material present within pores and on particle exterior surfaces (i.e. sand and CEM-II) increased with VA dosage. Furthermore, the levels of cementation and compaction present within the samples were at their optimum for the 25% CEM-II replacement mixtures. Increasing VA dosage from 25 to 50% had a significant effect on strength development, whereby it effectively introduced more unreactive filler material and reduced the cementitious binder content, as reflected in the CS data presented in Fig. 12.

Based on global observations for SBA-based mortars in Figs. 18b, d and f, increasing the SBA content from 10 to 50% had the effect of reducing the levels of cementation and particle packing, thereby increasing the number of

interconnected pore spaces. As a consequence, increasing SBA replacement dosages reduced CS values, which corroborates the CS data presented in Fig. 12.

Mineralogy

XRD spectra for the raw VA and SBA residues are presented in Fig. 19. These serve as a baseline for spectra produced for the 28-day cured VA and SBA-based mortars (Fig. 20). The spectra for VA is relatively simple; whereby it is chiefly characterised by a ‘broad hump’ feature over the 2θ range of 24° – 36° , indicating the presence of amorphous silicates. Furthermore, a peak is indicated to be present at $2\theta = 27^\circ$, which indicates the presence of Phillipsite — an aluminosilicate mineral (bound to metal ions, Na, K and Ca). Contrastingly, the XRD spectra for SBA is more complex; whereby Gehlenite, Akermanite, Wollastonite, Plagioclase and Phillipsite were the principal mineral phases identified. Gehlenite (Ca /Al silicates) and Akermanite (Ca/Mg silicates) are melilite minerals of the sorosilicate group, whereas Wollastonite (CaSiO_3) is an industrial mineral.

Since the XRD spectra for the pulverised VA and SBA were dominated by peaks corresponding to quartz, XRD analyses for CEM-II-SBA and CEM-II-VA mortars were undertaken in the absence of sand, to provide better insights into the mineralogical phases present (Fig. 20). XRD spectra produced for 28-day cured control, VA and SBA-based mortar mixtures, at 10%, 25% and 50% replacement are presented in Fig. 20. The main mineral phases that were commonly present within all samples were Calcite (CaCO_3) originally present in cement, Portlandite ($\text{Ca}(\text{OH})_2$) and calcium silicate phases produced after hydration, Alite ($3\text{CaO}\cdot\text{SiO}_2$) (C_3S), which forms large euhedral pseudo-hexagonal crystals and makes up the dominant part of Portland cement and Belite silicate ($2\text{CaO}\cdot\text{SiO}_2$) (C_2S), which originates from Portland cement clinkers. One of the key differences between spectra for VA and SBA samples was the presence of a peak at $2\theta = 31^\circ$ within SBA mixtures, which corresponds to Ca /Al and Ca/Mg silicates present in the SBA residues (Fig. 19). The amorphous content of the cured mortar mixtures was negligible, given the absence of the ‘amorphous hump’ [39].

Microstructural Bonding Characterisation

To confirm the nature of cementitious products that formed within the matrices of the controlled, VA and SBA-based mortars as a result of hydration and pozzolanic reactions, FTIR analyses were undertaken. Presented in Fig. 21 are transmittance spectra for CEM-II (C), CEM-II + sand (CS), CEM-II + sand + water (CSW) and 28-day water cured CEM-II + sand + water mix (cured CSW), which serve as

Fig. 14 Mechanical behaviour of VA-based mortar mixes: 25% replacement + 2% extra water at **a** 7-days and **b** 28-days; SBA-based mortar mixes 25% replacement + 2% extra water at **c** 7-days and **d** 28-days

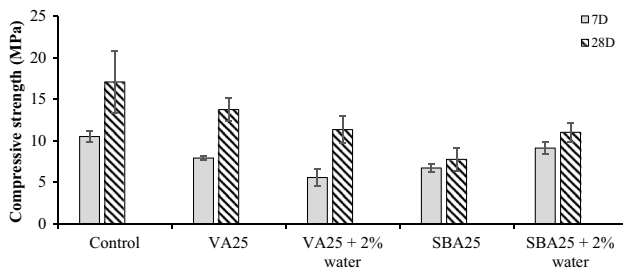
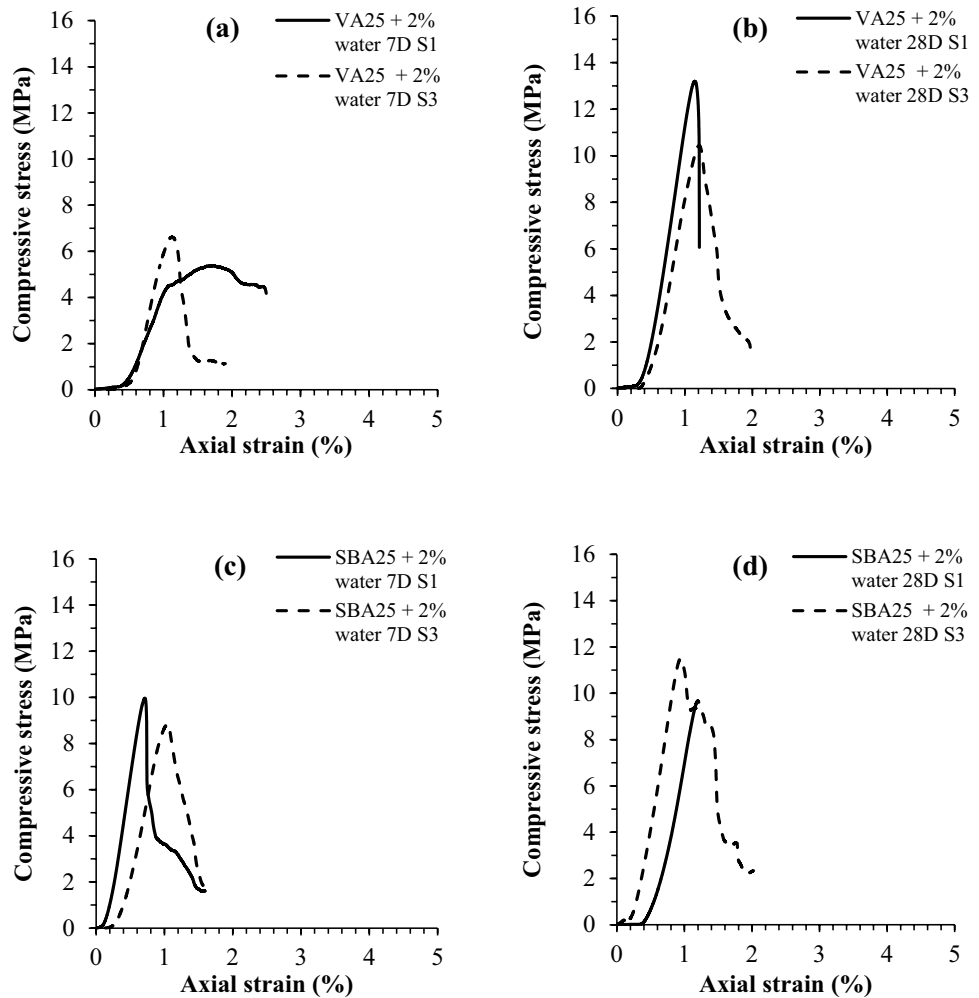


Fig. 15 Summary of 7-day and 28-day CS performances for control, VA and SBA-based mortar mixtures at 25% replacement + 2% extra water

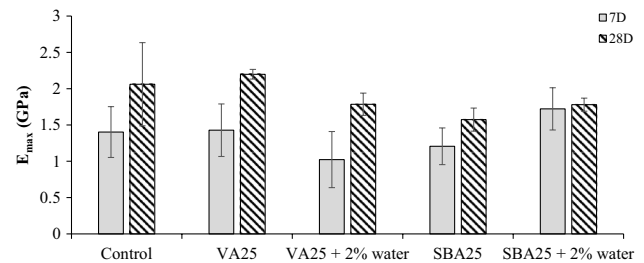


Fig. 16 Summary of 7-day and 28-day E_{max} values for control, VA and SBA-based mortar mixtures at 25% replacement + 2% extra water

reference spectra to reflect the evolution of mortars over 28-days.

Table 3 summarises the peaks corresponding to CO_3^{2-} anion of CaCO_3 , which formed through the carbonation of CaO in CEM-II. These peaks were mostly visible within the C and CSW mixes, whereby curing with hydration suppressed these peaks for the cured

mixture (cured CSW) spectrum. The broad peak within the $3200\text{--}3550\text{ cm}^{-1}$ range is indicative of intermolecular hydrogen bonds. The band for cured mix (cured CSW) shows new resolved peaks in this region compared with the fresh mortar mix (CSW), which reflects changes to the nature of hydroxyl groups after curing. Furthermore, this indicates the formation of novel hydrogen bonds and

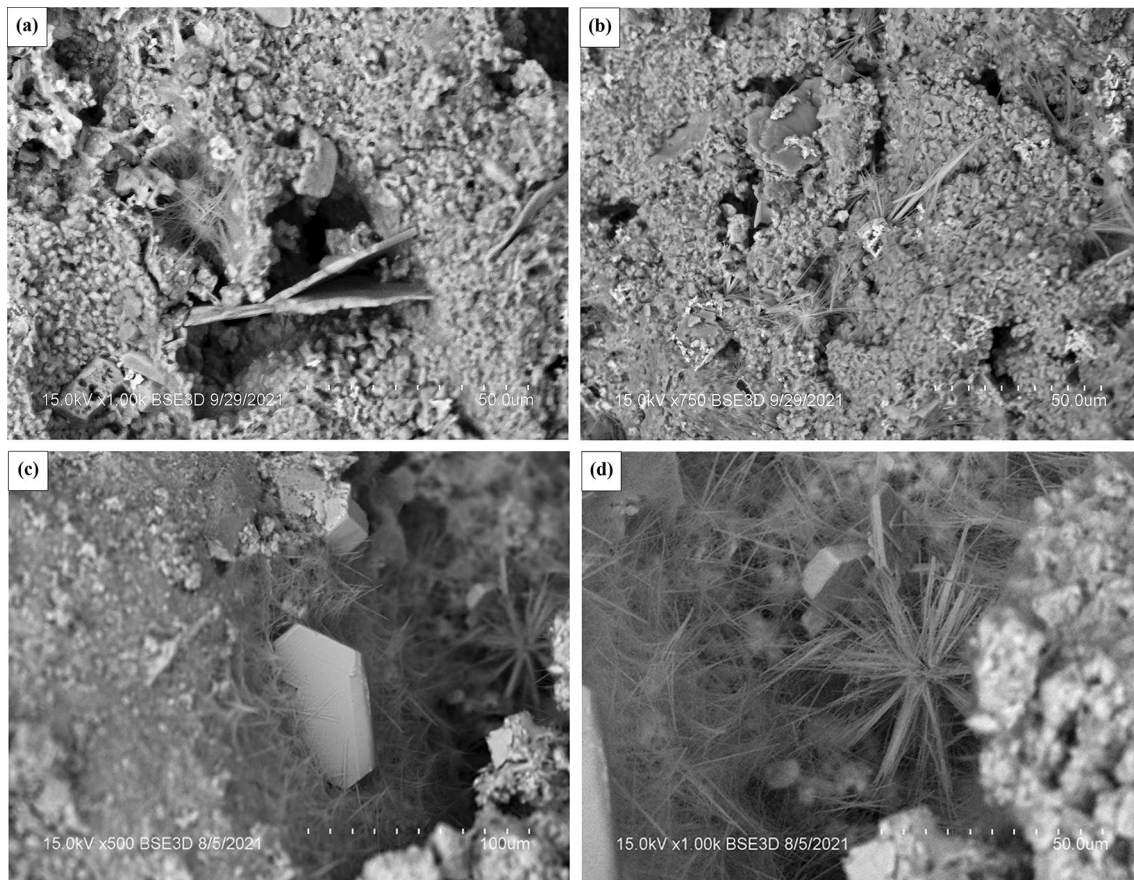


Fig. 17 SEM micrographs showing the microstructural characteristics of control CEM-II mortars cured for 28-days: **a** CH and ettringite phases within pore, **b** densely compacted and well-cemented struc-

ture, **c** CH and ettringite adhered to a sand particle, **d** extensive ettringite growth within a pore

changes in chemistry after hydration in the cement mortar, with the peak assignments listed in Table 3.

The new band of peaks present in the range of $1000\text{--}1250\text{ cm}^{-1}$ for the CSW and cured CSW spectra are indicative of calcium silicate hydrates (C–S–H) during cement hydration [33]. The observation of needle-like growths in the SEM micrographs of control mortars (Fig. 17d) are confirmed by characteristic FTIR peak at 1114 cm^{-1} for S–O bond (in sulphates) as ettringite.

FTIR spectra scanned in $450\text{--}4000\text{ cm}^{-1}$ wavenumber range for the raw VA and SBA residues are shown in Fig. 22. The peak at approximately 962 cm^{-1} in VA could be attributed to an asymmetric vibration of Si–OH (950 cm^{-1}) [44]. Furthermore, based on observations made by Beganskiene et al. [45], the band present in the range $800\text{--}1260\text{ cm}^{-1}$ for both VA and SBA spectra is likely to be a superimposition of different SiO_2 peaks.

The FTIR spectra for the 28-day pastes (without sand) containing 10, 25 and 50% replacement of CEM-II with VA and SBA are shown in Fig. 23. A diminished transmittance peak at 1406 cm^{-1} (corresponding to asymmetric stretching

of the CO_3^{2-} anion) was observed, compared with the peak observed at 1000 cm^{-1} (associated with the peak for asymmetric stretching mode of Si–O–Si), due to the addition of the VA and SBA residues. This may be due to $\text{Ca}(\text{OH})_2$ consumption by the residues, which fuelled the reaction of CaCO_3 to $\text{Ca}(\text{OH})_2$ conversion to form cement hydration products. No spectral changes were observed upon the adding 2% extra water to 25% SBA and VA mixtures as the bond chemistry was not affected.

Discussion

Reheating VA during LOI testing resulted in the formation of fused particulate and a glassy microstructure, thereby increasing the Si content to 22%. Unlike VA, a slight mass gain was observed for SBA at temperatures $> 600\text{ }^\circ\text{C}$ during TGA testing. This demonstrates the inability of VA to oxidise compared with SBA. Whilst LOI values of $< 0.3\%$ indicate high inorganic contents for both residues, SBA was slightly more alkali compared with VA, which could

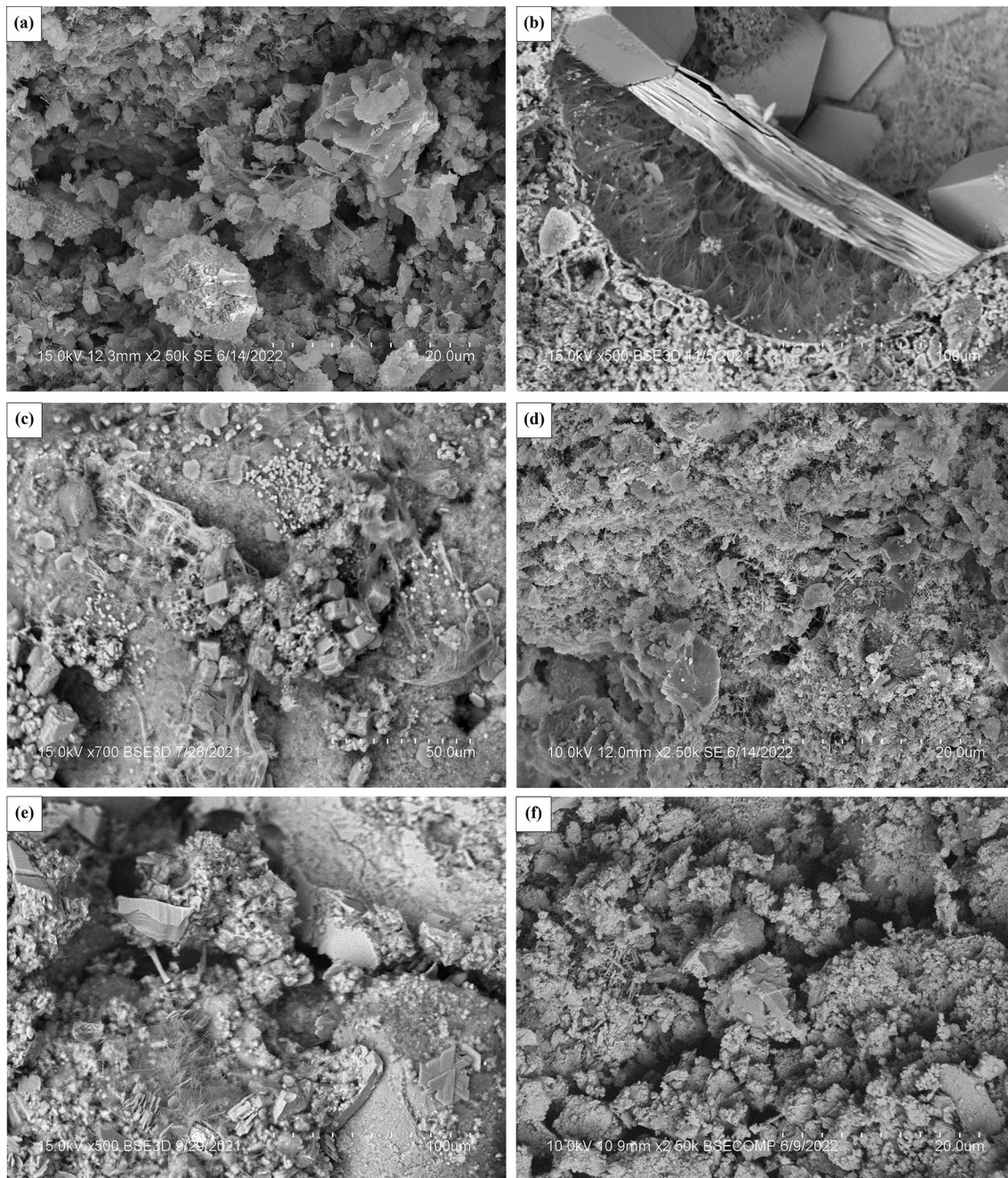


Fig. 18 Microstructure of 28-day cured CEM-II mortars replaced with 10% **a** VA, **b** SBA; 25%, **c** VA, **d** SBA; and 50% (**e**) VA and **f** SBA

be attributed to VA's reduced ability to hydrate due to its vitrified structure.

Whilst the pozzolanic activity of SBA and VA were not too dissimilar, with CaO removals of 55% and 51% respectively; mortars containing SBA produced higher mechanical strengths when using lower levels (10%) of CEM-II replacement in contrast with VA-based mixtures. Increasing residue content towards 25% replacement resulted in strength reductions for SBA-based mortar mixtures, and strength

enhancement for VA-based mixes. Hence, the mechanisms through which VA and SBA-based mortars developed strength were different; whereby VA particles acted as: 1) an additional source of silica for forming new cementitious products and 2) an aggregate providing a 'micro-filler effect'. This corroborates findings by Goldman and Bentur [6] in that the micro-filler effect is the primary strengthening mechanism in concretes and mortars. However, increasing residue content to 50% CEM-II replacement (regardless of it

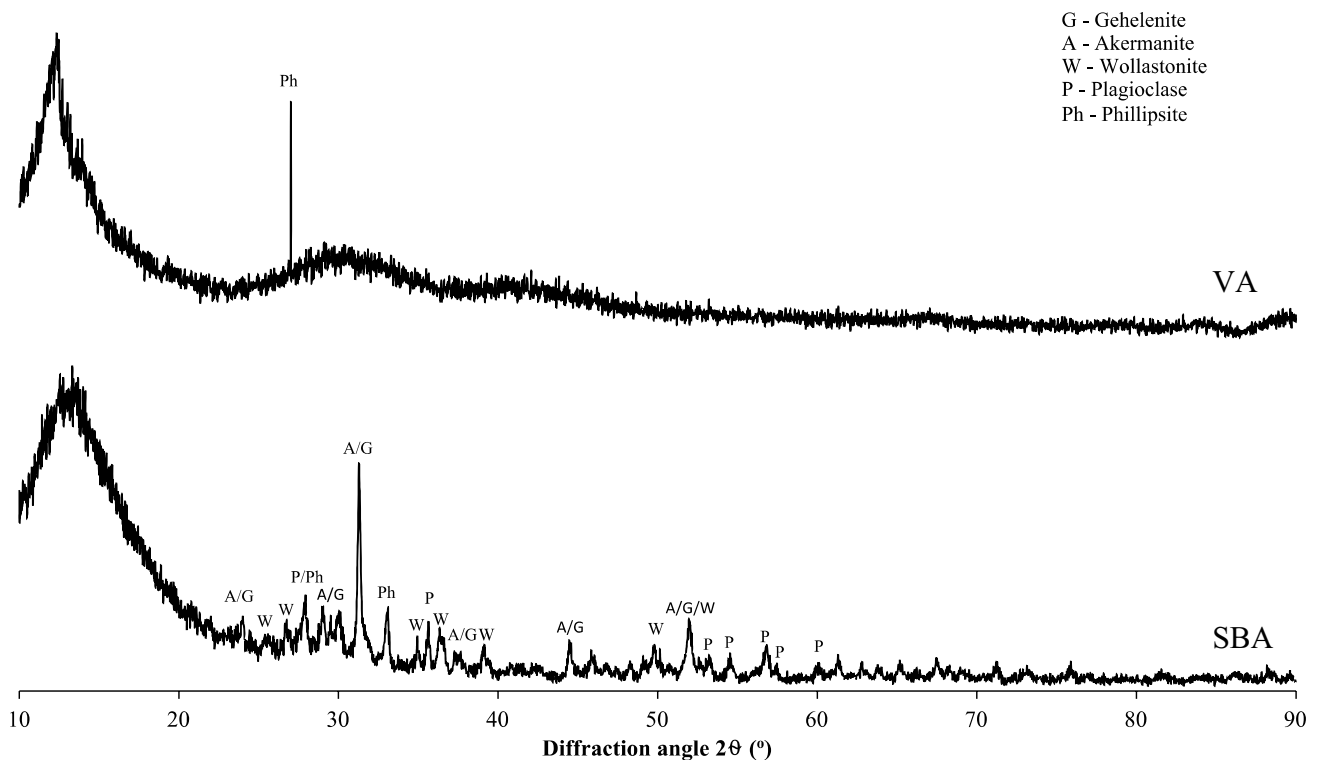


Fig. 19 XRD patterns for the pulverised VA and SBA residues

being VA or SBA) resulted in lower strengths compared with using 10% replacement and control mortars. VA50 samples produced markedly lower 7- and 28-day CS compared with SBA50 samples. At these higher levels of replacement, the strengths recorded were more influenced by the residue reactivity rather than micro-filler effects.

The 28-day CS values achieved by VA and SBA mortar designs were consistently lower (by 21–76%) than the control mortar, which achieved CS of 17.06 MPa after 28-days. These results are considered low for CEM-II based mortars. This can be attributed to the CS testing method adopted, whereby tests were performed using strain rate control rather than load rate control. Whilst this was very helpful in providing detailed insights into the stress–strain response (including creep) and failure mechanisms for the VA and SBA mortars, the CS results are considered to be moderately conservative and would be higher if cubic samples were tested using load rate control.

Additional strength gains observed in 25% SBA samples containing an extra 2% water suggests that the water absorption and retention behaviour of SBA would promote hydration reactions with curing beyond 28-days. A similar observation was made by Dixit et al. [46] for CEM-I-based mortars containing biochar as a replacement agent.

The original organic and chloride contents of the MSW feedstock (potentially representing sources of pollution) did not impact strength development of mortars, due to their

combustion during MSW incineration [32]. However, the VA and SBA residues contained relatively low concentrations of heavy metals including Cr, Zn and Fe. Whilst the concentrations of Cr and Zn were not of concern in terms of environmental pollution or interference with strength development, the Fe content may have played a role in the cementitious reactions. The role of Fe in strength development of cementitious materials is unclear. Evidence reported by Lemougna et al. [47] indicates that Fe retards strength development (due to its higher reactivity compared with Si and Al). Conversely, Ngintedem et al. [48] determined that increasing Fe content of binders up to 20% can produce higher strength gains. Since the Fe contents of SBA and VA were markedly higher than CEM-II, PFA and GGBS (as reported in Table 2), it is hypothesised that Fe had a detrimental role in CS performance — particularly for SBA based mortars as it has been demonstrated that SBA is more reactive than VA as an SCM.

Conclusions and Recommendations

This study investigated the mechanical behaviour, physico-chemical (pozzolanic) properties, mineralogy and micro-structure for a new set of circular economy-friendly cementitious mortars, which valorise thermally treated MSW as an SCM (rather than aggregate as previously investigated

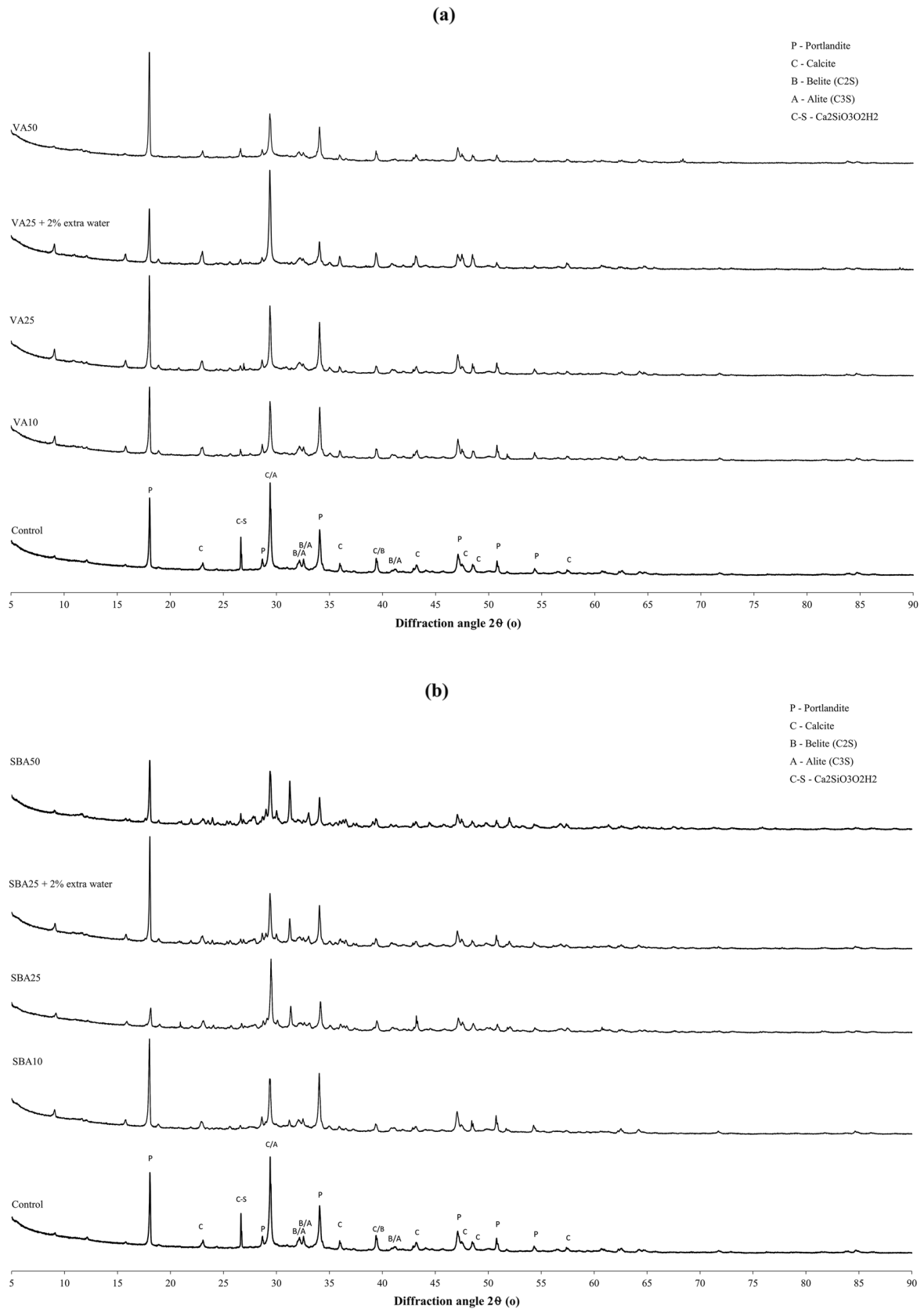


Fig. 20 XRD spectra for **a** VA, **b** SBA based paste mixes without sand after 28-days curing

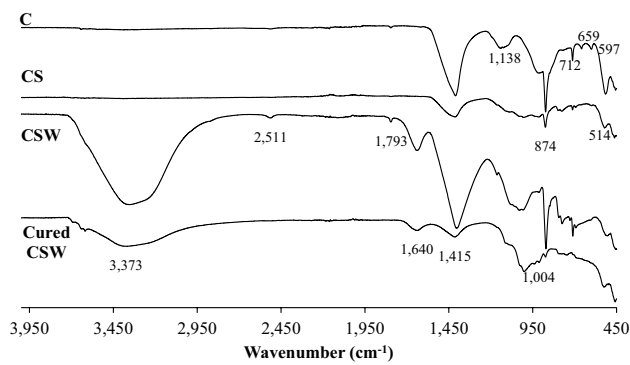


Fig. 21 FTIR spectra for CEM-II, sand and water constituents, and once mixed and cured for 28-days

by researchers). The following concluding remarks can be drawn from the experimental results presented in this study:

- MSW feedstocks treated at high temperatures (~ 1200 °C) with high inorganic contents ~ 99% may be used as SCMs in composite mortars at replacement dosages up to 50%. However, the optimum dosage is dependent on the phys-

ico-chemical characteristics of the incinerated MSW residues.

- SBA and VA were successfully used to replace CEM-II at dosages of 10 and 25% respectively without compromising the mechanical strength of the mortar. The use of 2% additional water in mortar designs containing 25% SBA improved strength performance, indicating that SBA's water retention properties permitted the precipitation of more hydration products and strength gains with curing.
- Using higher levels (50%) of CEM-II replacement with VA or SBA resulted in strength reductions, albeit strengths were higher when using 50% SBA over 50% VA. Overall, SBA had more prospects as an SCM for CEM-II compared with VA. Whilst VA and SBA exhibited comparable levels of pozzolanic activity, the slightly higher pH of SBA makes it more attractive over VA. Therefore, the pH of an MSW residue can provide initial insights into the solubility of metal ions and the reactivity of the material.
- Neutral pH values measured for VA were related to its vitrified form and high siliceous content. Additional water in the mortar mixtures increased strength gains in

Table 3 Peak assignments for FTIR spectra

IR absorption band (cm ⁻¹)	Assignment	Reference peak position (cm ⁻¹) [reference]
874; 852	(ν_2) out of plane bend/deformation of CO ₃ ²⁻ anion	876; 849 [40]
712	(ν_4) in plane bend/deformation of CO ₃ ²⁻ anion	714 [40]
1415	(ν_3) asymmetric stretching of CO ₃ ²⁻ anion	1458 [40] 1410 [41]
1793; 2511	Overtone of 874 cm ⁻¹ peak for out of plane bend/deformation of CO ₃ ²⁻ anion	1794; 2500–2980 [40]
3618	Stretching vibration of internal OH ⁻ groups for Al–O–H in aluminosilicates	3618 [42]
3641	Out-of-plane stretching vibrations of internal OH ⁻ associated with unreacted Ca(OH) ₂	3641 [40]
3694	Internal surface-free O–H stretching for Al–O–H (in-phase symmetric stretching) in aluminosilicates	3694 [42, 43]
514	Si–O vibrations in clinker phase Ca ₂ SiO ₄ (C ₂ S) Si–O (unassigned fundamentals) vibrations in clinker phase C ₂ S Fe–O (unassigned fundamentals) vibrations in clinker phase C ₄ AF Al–O (unassigned fundamentals) vibrations in clinker phase C ₃ A	518 [41] 509 [40] 500–700 region [40] 506 [40]
524	Si–O (unassigned fundamentals) vibrations in clinker phase C ₃ S	520 [40] 522 [41]
657; 598	ν_4 of Syngenite (sulphates) (bands for sulphates generally appear 50 cm ⁻¹ apart)	604; 658 [38]
1644	(ν_2) H–O–H bending in water	1600–1700 [44]
776 and 795 double band	Si–O–Si symmetric stretching vibrations	778 and 792 double band [38]
910	Al–O–H stretching Si–O asymmetric stretching mode of Si–O–Si	909 [42] 911 [41]
939	Si–O (unassigned fundamentals) vibrations in clinker phase Ca ₃ SiO ₅ (C ₃ S)	935 [40] 938 [41]
1000	Asymmetric stretching mode of Si–O–Si	1005 [42] 1001 [41]
1029	Asymmetric stretching mode of Si–O–Si	1029 [42]
1114	S–O stretching in sulphates in Ettringite Ca ₆ Al ₂ (SO ₄) ₃ (OH) ₁₂ /26H ₂ O	1115 [41]

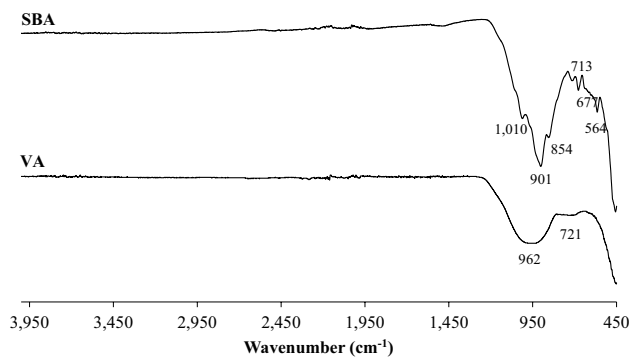


Fig. 22 FTIR for the pulverised VA and SBA residues

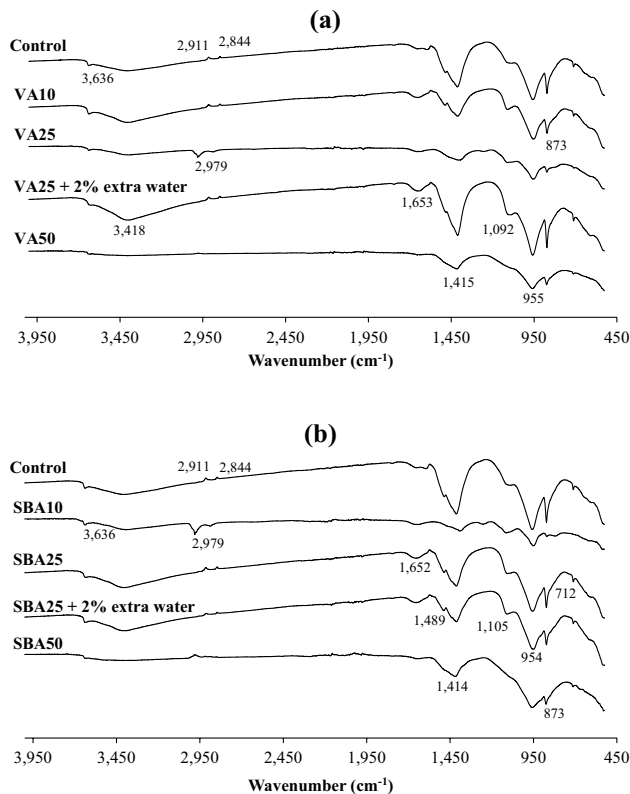


Fig. 23 FTIR spectra for 28-day cured mortar mixes (without sand) prepared with 10, 25 and 50% **a** VA and **b** SBA

SBA based mortars but not in VA based mortars. This indicated that VA served as a filler in the mortar whilst SBA acted as a reactive binder. Furthermore, since mortars containing 25% VA achieved higher strengths compared with 25% SBA, this indicates that at an equivalent dosage, the VA's micro-filler effect was more significant in promoting strength development over SBA's level of cementitious reactivity.

- FTIR analyses indicated that both VA and SBA-based mortars experienced depletions in CaCO_3 with

increased residue dosage, indicating consumption of the $\text{Ca}(\text{OH})_2$ by the residues to form new silicate hydrates. Of the CEM-II replacement dosages considered, 25% was the optimum for achieving the highest strengths. This suggests that there are further mechanisms affecting strength gain in addition to pozzolanic activity of SCMs.

There are numerous recommendations for performing future works to expand upon the findings of this study. Further long-term compressive strength, flexural strength, durability and leachate testing of the mortars will be required, whereby SBA will be used as an SCM and VA as a supplementary or replacement sand aggregate. Bound water measurements are understood to correlate well with mechanical strength in cementitious mixtures [49], and therefore warrants investigation to determine pozzolanic activity of SBA in future studies. Moreover, the water retention capacity of SBA as an SCM also requires investigation to quantify the amount of physically bound water that can participate in hydration and pozzolanic reactions during wet and air curing. Finally, an environmental assessment (e.g. life cycle analysis, involving a cradle-to-cradle approach) of the hybrid CEM-II + SBA / VA mortars is necessary to confirm that the use of these waste materials in mortars aligns with governmental and industrial net zero carbon emission agendas.

Acknowledgements The authors would like to thank REWS UK for providing SBA and VA residue samples, along with information regarding their generation.

Authors Contributions All authors contributed to the study conception and design. Material preparation, data collection and analysis were performed by DAW, PS, DJH and CJE. The first draft of the manuscript was written by DAW, with a detailed review performed by Paul Sargent on previous versions of the manuscript. All authors approved the final manuscript.

Funding This research was funded by the European Regional Development Fund (ERDF) (Ref. No. 34R17P02148) and Scott Bros Ltd, Billingham, UK.

Availability of Data and Materials All raw and processed data / materials will be made available by the authors on request.

Declarations

Competing interests The authors have no relevant financial or non-financial interests to disclose.

Ethical Approval The authors confirm that the content of this manuscript (results, data, figures, text) has not been published elsewhere, nor is it under consideration by another publisher. The work presented is original and has been approved by Teesside University's research ethics committee. All of the material presented in this manuscript is owned by the authors. No permissions required.

Consent to Participate Not applicable (no human or animal participation was involved in this work).

Consent for Publication All authors agreed with the content of the manuscript. All authors and their respective institutions gave consent to submit this manuscript.

Open Access This article is licensed under a Creative Commons Attribution 4.0 International License, which permits use, sharing, adaptation, distribution and reproduction in any medium or format, as long as you give appropriate credit to the original author(s) and the source, provide a link to the Creative Commons licence, and indicate if changes were made. The images or other third party material in this article are included in the article's Creative Commons licence, unless indicated otherwise in a credit line to the material. If material is not included in the article's Creative Commons licence and your intended use is not permitted by statutory regulation or exceeds the permitted use, you will need to obtain permission directly from the copyright holder. To view a copy of this licence, visit <http://creativecommons.org/licenses/by/4.0/>.

References

- De Brito, J., Evangelista, L., Silvestre, J.D.: Equivalent functional unit in recycled aggregate concrete, pp. 293–327. In: De Brito, J., Agrela, F. (Eds.), *New Trends in Eco-efficient and Recycled Concrete*. San Diego: Elsevier Science and Technology (2019). ISBN: 9780081024805.
- Rodriguez-Robles, D., Van den Heede, P., De Belie, N.: Life cycle assessment applied to recycled aggregate concrete, pp. 207–256, in De Brito, J. and Agrela, F. (Eds.), *New Trends in Eco-efficient and Recycled Concrete* (2019). San Diego: Elsevier Science and Technology. ISBN: 9780081024805. <https://doi.org/10.1016/B978-0-08-102480-5.00009-9>.
- Chatham House Report.: *Making Concrete Change: Innovation in Low-carbon Cement and Concrete* (2018). <https://reader.chathamhouse.org/making-concrete-change-innovation-low-carbon-cement-and-concrete>. Accessed 10th Dec 2020
- Grabiec, A.M., Zawal, D., Razaq, W.A.: The effect of curing conditions on selected properties of recycled aggregate concrete. *Appl. Sci.* **10**(13), 4441 (2020). <https://doi.org/10.3390/app10134441>
- Environment, U.N., Scrivener, K.L., John, V.M., Gartner, E.M.: Eco-efficient cements: potential economically viable solutions for a low-CO₂ cement-based materials industry. *Cem. Concr. Res.* **114**, 2–26 (2018). <https://doi.org/10.1016/j.cemconres.2018.03.015>
- Goldman, A., Bentur, A.: Properties of cementitious systems containing silica fume or nonreactive microfillers. *Adv. Cem. Based Mater.* **1**(5), 209–215 (1994). [https://doi.org/10.1016/1065-7355\(94\)90026-4](https://doi.org/10.1016/1065-7355(94)90026-4)
- DEFRA.: Department for Environment Food and rural affairs—*Incineration of Municipal Solid Waste*, February 2013. (2023) https://assets.publishing.service.gov.uk/government/uploads/system/uploads/attachment_data/file/221036/pb13889-incineration-on-municipal-waste.pdf. Accessed 16 Jun 2022.
- GOV.UK.: UK energy in brief. (2022) https://assets.publishing.service.gov.uk/government/uploads/system/uploads/attachment_data/file/1130451/UK_Energy_in_Brief_2022.pdf. Accessed 20 Apr 2023.
- Tang, P., Florea, M.V.A., Spiesz, P., Brouwers, H.J.H.: Characteristics and application potential of municipal solid waste incineration (MSWI) bottom ashes from two waste-to-energy plants. *Constr. Build. Mater.* **83**, 77–94 (2015). <https://doi.org/10.1016/j.conbuildmat.2015.02.033>
- Xuan, D., Tang, P., Poon, C.S.: Limitations and quality upgrading techniques for utilization of MSW incineration bottom ash in engineering applications—a review. *Constr. Build. Mater.* **190**, 1091–1102 (2018). <https://doi.org/10.1016/j.conbuildmat.2018.09.174>
- Loginova, E., Volkov, D.S., van de Wouw, P.M.F., Florea, M.V.A., Brouwers, H.J.H.: Detailed characterization of particle size fractions of municipal solid waste incineration bottom ash. *J. Clean. Prod.* **207**, 866–874 (2019). <https://doi.org/10.1016/j.jclepro.2018.10.022>
- Tang, P., Chen, W., Xuan, D., Zuo, Y., Poon, C.S.: Investigation of cementitious properties of different constituents in municipal solid waste incineration bottom ash as supplementary cementitious materials. *J. Clean. Prod.* **258**, 120675 (2020). <https://doi.org/10.1016/j.jclepro.2020.120675>
- Thenarasanan Latha, A., Murugesan, B., Thomas, B.S.: Compressed stabilized earth block incorporating municipal solid waste incinerator bottom ash as a partial replacement for fine aggregates. *Buildings (Basel)* **13**(5), 1114 (2023). <https://doi.org/10.3390/buildings13051114>
- Abinaya, T.L., Balasubramanian, M.: Department of Civil Engineering, SRM Institute of Science and Technology, India & School of Architecture and Interior Design, SRM Institute of Science and Technology, India 2022. A circular economy in waste management carrying out experimental evaluation of compressed stabilized earth block using municipal solid waste incinerator fly ash. *Mağallaṭ al-abḥaṭh al-handasiyyaṭ*, Vol. 9. <https://doi.org/10.36909/jer.ACMM.16319>.
- Yang, Z., Ji, R., Liu, L., Wang, X., Zhang, Z.: Recycling of municipal solid waste incineration by-product for cement composites preparation. *Constr. Build. Mater.* **162**, 794–801 (2018). <https://doi.org/10.1016/j.conbuildmat.2017.12.081>
- Li, X., Lv, Y., Ma, B., Chen, Q., Yin, X., Jian, S.: Utilization of municipal solid waste incineration bottom ash in blended cement. *J. Clean. Prod.* **32**, 96–100 (2012). <https://doi.org/10.1016/j.jclepro.2012.03.038>
- Caprai, V., Gauvin, F., Schollbach, K., Brouwers, H.J.H.: MSWI bottom ash as binder replacement in wood cement composites. *Constr. Build. Mater.* **196**, 672–680 (2019). <https://doi.org/10.1016/j.conbuildmat.2018.11.153>
- Bethanis, S., Cheeseman, C.R., Sollars, C.J.: Properties and microstructure of sintered incinerator bottom ash. *Ceram. Int.* **28**(8), 881–886 (2002). [https://doi.org/10.1016/S0272-8842\(02\)00068-8](https://doi.org/10.1016/S0272-8842(02)00068-8)
- Alam, Q., Florea, M.V.A., Schollbach, K., Brouwers, H.J.H.: A two-stage treatment for Municipal Solid Waste Incineration (MSWI) bottom ash to remove agglomerated fine particles and leachable contaminants. *Waste Manag.* **67**, 181–192 (2017). <https://doi.org/10.1016/j.wasman.2017.05.029>
- Cheeseman, C.R., Makinde, A., Bethanis, S.: Properties of lightweight aggregate produced by rapid sintering of incinerator bottom ash. *Resour. Conserv. Recycl.* **43**(2), 147–162 (2005). <https://doi.org/10.1016/j.resconrec.2004.05.004>
- Geetha, S., Ramamurthy, K.: Properties of sintered low calcium bottom ash aggregate with clay binders. *Constr. Build. Mater.* **25**(4), 2002–2013 (2011). <https://doi.org/10.1016/j.conbuildmat.2010.11.051>
- Risnandani, P., Jaya Ekaputri, J., Maulidiyawati, I., Puspitasari, P.: Mechanical properties of concrete composed of sintered fly lightweight aggregate. *MATEC Web Conf.* **195**, 1008 (2018)
- Concrete Centre.: Embodied CO₂ e of UK cement, additions and cementitious material [online]. https://www.concretecentre.com/TCC/media/TCCMediaLibrary/Products/Factsheet_18_2019_updateF.pdf. Last Accessed 27 Sept 2023.
- British Standards Institution (BSI): BS 197-1, Cement. Composition, specifications and conformity criteria for common cements. British Standards Institution, Milton Keynes (2011)

25. Zhang, H.: Building materials in civil engineering. Woodhead Publishing, Cambridge (2011) 978-1-84569-955-0
26. Ghiasvand, E., Ramezani-pour, A.A., Ramezani-pour, A.M.: Effect of grinding method and particle size distribution on the properties of Portland-pozzolan cement. *Constr. Build. Mater.* **53**, 547–554 (2014). <https://doi.org/10.1016/j.conbuildmat.2013.11.072>
27. British Standards Institution (BSI): BS EN 12620:2002+A1:2008, Aggregates for concrete. British Standards Institution, Milton Keynes (2002)
28. British Standards Institute (BSI): BS 1377-2, Methods of Test for Soils for Civil Engineering Purposes. British Standards Institution, Milton Keynes (2022)
29. American Standard Testing Manual (ASTM): ASTM E1131-20 ISO 11358, Standard test method for compositional analysis by thermogravimetry (2020). <https://doi.org/10.1520/E1131-20>
30. Donatello, S., Tyrer, M., Cheeseman, C.R.: Comparison of test methods to assess pozzolanic activity. *Cem. Concr. Compos.* **32**(2), 121–127 (2010). <https://doi.org/10.1016/j.cemconcomp.2009.10.008>
31. British Standards Institute (BSI), 2016. BS EN 196-1:2016: Methods of testing cement. Determination of strength. British Standards Institution, Milton Keynes.
32. Cao, W., Li, J., Zhang, X.: Evaluation of the effects and interactions of initial chlorine and sulphur contents on the release of potassium compounds during biomass combustion. *J. Energy Inst.* **101**, 178–186 (2022). <https://doi.org/10.1016/j.joei.2022.01.014>
33. Gonzalez, J., Sargent, P., Ennis, C.: Sewage treatment sludge biochar activated blast furnace slag as a low carbon binder for soft soil stabilisation. *J. Clean. Prod.* **311**, 127553 (2021). <https://doi.org/10.1016/j.jclepro.2021.127553>
34. Mahima Kumar, M., Senthilvadivu, R., Brahmaji Rao, J.S., Neelamegam, M., Ashok Kumar, G.V.S., Kumar, R., Jena, H.: Characterization of fly ash by ED-XRF and INAA for the synthesis of low silica zeolites. *J. Radioanal. Nucl. Chem.* **325**, 941–947 (2020). <https://doi.org/10.1007/s10967-020-07243-0>
35. Agarwal, S.K.: Pozzolanic activity of various siliceous materials. *Cem. Concr. Res.* **36**(9), 1735–1739 (2006). <https://doi.org/10.1016/j.cemconres.2004.06.025>
36. Provis, J.L., van Deventer, J.S.J.: Geopolymers: Structure, processing, properties and industrial applications (2009). Woodhead Publishing Ltd. ISBN 978-1-84569-638-2
37. Davidson, L.K., Demirel, T., Handy, R.I.: Soil pulverization and lime migration in soil lime stabilization. *Highway Res. Rec.* **1965**(92), 103–126 (1965)
38. Liu, Y., Zeng, F., Sun, B., Jia, P., Graham, I.T.: Structural characterizations of aluminosilicates in two types of fly ash samples from Shanxi Province, North China. *Minerals* **9**(6), 358 (2019). <https://doi.org/10.3390/min9060358>
39. Provis, J.L.: Modelling the formation of geopolymers. PhD thesis submitted to The University of Melbourne (2006). <https://rest.neptune-prod.its.unimelb.edu.au/server/api/core/bitstreams/8c9ef47b-3944-57cf-acdf-70c3902846ad/content>
40. Hughes, T.L., Methven, C.M., Jones, T.G.J., Pelham, S.E., Fletcher, P., Hall, C.: Determining cement composition by Fourier transform infrared spectroscopy. *Adv. Cem. Based Mater.* **2**(3), 91–104 (1995). [https://doi.org/10.1016/1065-7355\(94\)00031-X](https://doi.org/10.1016/1065-7355(94)00031-X)
41. Horgnies, M., Chen, J., Bouillon, C.: Overview of the use of Fourier Transformed Infrared Spectroscopy to study cementitious materials. *WIT Trans. Eng. Sci.* **77**(10), 2495/MC130221. <https://doi.org/10.2495/MC130221>
42. Sarma, J., Rajkhowa, S., Mahiuddin, S.: Upgradation of iron ore fines and slime by selective flocculation using surface-active agents, settling study, and characterization of the beneficiation waste for value addition. *J. Chem.* (2022). <https://doi.org/10.1155/2022/6451187>
43. Farmer, V.C.: Transverse and longitudinal crystal modes associated with OH stretching vibrations in single crystals of kaolinite and dickite. *Spectrochim. Acta Part A* **56**(5), 927–930 (2000). [https://doi.org/10.1016/S1386-1425\(99\)00182-1](https://doi.org/10.1016/S1386-1425(99)00182-1)
44. Suman, L.S.: Characterization of some cement samples of Nepal using FTIR spectroscopy. In: International Journal of Advanced Research in Chemical Science (IJARCS), Vol. 5, No. 7. pp. 19–23 (2018). <https://doi.org/10.20431/2349-0403.0507004>
45. Beganskienė, A., Sirutkaitis, V., Kurtinaitienė, M., Juškėnas, R., Kareiva, A.: FTIR, TEM and NMR investigations of stöber silica nanoparticles. *Mater. Sci.* **10**:287–290(2004).
46. Dixit, A., Gupta, S., Pang, S.D., Kua, H.W.: Waste valorisation using biochar for cement replacement and internal curing in ultra-high-performance concrete. *J. Clean. Prod.* **238**, 117876 (2019). <https://doi.org/10.1016/j.jclepro.2019.117876>
47. Lemougna, P.N., MacKenzie, K.J.D., Jameson, G.N.L., Rahier, H., Chinje Melo, U.F.: The role of iron in the formation of inorganic polymers (geopolymers) from volcanic ash: a ⁵⁷Fe Mössbauer spectroscopy study. *J. Mater. Sci.* **48**, 5280–5286 (2013). <https://doi.org/10.1007/s10853-013-7319-4>
48. Ngnintedem, D.L.V., Lampe, M., Tchakouté, H.K., Rüscher, C.H.: Effects of iron minerals on the compressive strengths and microstructural properties of Metakaolin-based geopolymer materials. *Gels* **8**(8), 525 (2022). <https://doi.org/10.3390/gels8080525>
49. Li, X., Snellings, R., Antoni, M., Alderete, N.M., Ben Haha, M., Bishnoi, S., Cizer, Ö., Cyr, M., De Weerd, K., Dhandapani, Y., Duchesne, J., Haufe, J., Hooton, D., Juenger, M., Kamali-Bernard, S., Kramar, S., Marroccoli, M., Mary Joseph, A., Parashar, A., Patapy, C., Provis, J.L., Sabio, S., Santhanam, M., Steger, L., Sui, T., Telesca, A., Vollpracht, A., Vargas, F., Walkley, B., Winnefeld, F., Ye, G., Zajac, M., Zhang, S., Scrivener, K.L.: Reactivity tests for supplementary cementitious materials: RILEM TC 267-TRM phase 1. *Mater. Struct.* **51**, 151 (2018). <https://doi.org/10.1617/s11527-018-1269-x>

Publisher's Note Springer Nature remains neutral with regard to jurisdictional claims in published maps and institutional affiliations.